# Formation of Patterns in Granular Materials

André Betat[1], Christian M. Dury[2], Ingo Rehberg[1], Gerald H. Ristow[2], Michael A. Scherer[1], Matthias Schröter[1], and Gunther Straßburger[1]

[1] Otto–von–Guericke–Universität Magdeburg, Postfach 4120, D-39016 Magdeburg, Germany
[2] Philipps–Universität Marburg, Fachbereich Physik, Renthof 6, D-35032 Marburg, Germany

**Abstract.** In order to study the behaviour of fluidized granular material experimentally and numerically, we propose to investigate pattern–forming processes, because they can be easily observed and quantitatively characterized. We report measurements on five such systems, namely pattern formation of granular material i) by segregation, under the influence of ii) linear horizontal and iii) circular horizontal vibration, iv) water shear flow, and in v) a sedimenting suspension.

## 1 Introduction

Sand, when considered as a continuum, is an unusal one: Under some circumstances it behaves like a fluid, as is best demonstrated in a hour–glass. A stable pile of sand, on the other hand, demonstrates the limitations of this point of view: It does not flow apart. At present, a theoretical description of these two aspects or related peculiar behaviour of granular matter cannot be condensed into a coherent theoretical model (for a recent review see Jaeger et al. (1996b)). In order to describe granular flow, several complementary methods are currently being used. For sufficiently low densities and a sufficiently fast motion of the granulate, a hydrodynamic description is possible. Throughout the last few years, numerical methods have been successful in modelling the collective behaviour on a limited number of particles. In this chapter we will focus on those methods, and a number of experiments suitable for testing the limitations of theoretical models.

All the theoretical models rely on simplifications of the interaction of the grains. Thus, experimental tests are crucial. For some of the experiments presented in this chapter, such a test is indeed the primary motivation. The experimental difficulties of granular matter are due to the uncontrolled surface of the granulate, the influence of humidity, and the uncontrolled charging of the particles. Considering these difficulties it seems already a challenge in its own to find paradigmatic experimental systems that are suitable for a quantitative comparison with theoretical approaches describing granular material. The present chapter describes two systems which have this property: The problem of humidity and charging can either be overcome by using comparatively large particles, or by using a suspension of sand in water. Many of

the experiments described below were chosen because we feel that they have a strong potential for clarifying fundamental questions concerning granular matter. It is not the intention of this article to present an overview of solved problems, we rather hope that our presentation helps to stimulate further research.

The paper is organized in the following way: In section 2, we mention briefly some of the most striking observations concerning the statics of granular matter. In section 3, some aspects of the dynamics are described. Special emphasis is given to fluidization, the necessary precursor of dynamical behaviour. For fluidized granulate we concentrate on two aspects of the dynamics, namely segregation and the formation of surface patterns. This allows an elegant approach to measure the quantitites of interest, namely image processing. A short overview on the numerical methods used to describe granular matter is given in the appendix.

## 2 Statics of Granulate

The force distribution in a static arrangement of granular particles is of technical interest, for example in silos. Here, unlike in a fluid, the pressure at the bottom of the container is not proportional to the height of the material resting on top of it, instead it reaches a nearly constant value (Janssen 1895), because the walls can support the extra weight. This effect also explains to some extend why the flow rate in a hour–glass is almost constant. The force distribution inside the granulate has an interesting structure, in particular, it shows spatial fluctuations. The fact that a worm survives in sand even some meters below the surface, where the pressure would be much too high for a fluid-like behaviour, is a manifestation of those fluctuations. Another interesting example is the pressure distribution at the bottom of a sand heap: The maximum pressure does not seem to be in the middle of the heap, where the sand is highest. There is no simple way to model this behaviour theoretically: It is not possible to create a heap from monodisperse spheres, the existence of the sand heap, and in consequence the complicated force distribution, is due to the more complicated shape of the sand particles.

## 3 Dynamics of Granular Flow

The important difference between granular material and the more classical many-body systems considered in statistical physics is dissipation - the collisions between two sand particles are inelastic. Therefore granular matter is normally at rest, energy must be supplied to observe dynamical behaviour. Both in nature (avalanches) and in technical applications (silos) this is often just gravitational energy. In such cases the flow is only of transient nature and thus not very convenient for laboratory experiments. In spite of this nuisance, the sedimentation experiment described below falls into this class.

Rotation - as in the segregation experiment described below - or vibration are the most often used methods to supply energy continuously. In particular, vertical vibration seems to be a popular method (Bizon et al. 1998), while we concentrate on horizontal vibrations in the experiments described below. In the third class of experiments we provide the energy to the granulate by means of rotational shear flow. In all experiments, the external driving has to overcome a threshold for a transition from a solid–like to a fluid– or gas–like behaviour of the granulate to occur. We have examined this transition in detail only for the case of linear horizontal vibration, which will be described in the following subsection.

### 3.1 Fluidization of Granular Matter

One of the most fascinating properties of granular matter is their transition from a solid-like behaviour to a fluid-like behaviour (the so–called fluidization, see e.g. Esipov and Pöschel (1997)), which appears when increasing the strength of external shear or the acceleration of vibration (Clément and Rajchenbach 1991, Gallas et al. 1992). In most experiments, this transition seems easy to pinpoint by visual inspection of the granulate. However, a precise determination is not possible: individual grains do move both below and above the fluidization point. An objective order parameter suitable for measuring this fascinating transition from solid-like to fluid-like behaviour is necessary.

We studied this transition experimentally and by computer simulations for horizontal vibration of a granulate and proposed two such order parameters, one based on the so-called granular temperature, the other extracted from the pair distribution function (Ristow et al. 1997). By using these order parameters, we have been able to determine the scaling of the fluidization point, and find that it scales with the *acceleration* of the vibration. This behaviour was also observed for the threshold of the free surface instability (Evesque and Rajchenbach 1989) and the spontaneous heaping instability (Clément et al. 1992) in sand piles undergoing vertical vibrations. Interestingly enough, according to our numerical simulations, the granular temperature scales with the *velocity* of the vibration. We cannot explain this scaling, but note that it is reminiscent of the scaling for the height of the center of mass of a granulate under vertical vibration (Warr et al. 1995, Luding et al. 1994), or the scaling of the granular temperature (Warr et al. 1995, Lee 1995).

The experimental apparatus used for the horizontal vibration of granulate is described in Ristow et al. (1997). The available amplitude was in the range of 0 mm – 50 mm, and the frequency was from 0.9 Hz – 4.3 Hz. We used a channel of 100 mm length in the direction of the vibration, 0.6 mm width and 20 mm height. The container was filled with granular material consisting of commercially available glass beads. The particles were close to spherical. We have developed a method to get rid of the grains which deviate considerably from this shape, by making use of the different rolling behaviour of

spheres and non-spherical particles down an inclined plane. The diameter of the spheres was between 0.52 mm and 0.6 mm. The lower was determined by sieving, and the upper one by both a sieving procedure and the channel width. The channel was filled with a monolayer of spheres, and the height of the granulate was 3-5 particles, i.e. we use about 700 particles. No attempt was made to count this number exactly, because the solid-fluid transition seems to be fairly independent of the exact number. We used two methods to determine the particle motion.

By the first method the particle motion was measured in the co–moving frame by a CCD–camera connected to a frame grabber. The camera recorded the central 40 mm of the channel from the side, i.e. perpendicular to the direction of the oscillation. 32 snapshots were digitized with a sampling rate of 25 Hz. We obtained a binary image by giving pixels associated with the background a value of zero, and pixels associated with a particle the value of 1. In order to characterize the fluidization we subtracted consecutive binary images pixelwise, and took the mean square of the resulting difference. The resulting number is called *pixel change*. In order to obtain a temporal mean value over about one period of the driving, we took the mean value of about 7 (depending on the driving frequency) pixel changes. The resulting number is plotted in Fig. 1 as a function of the vibration frequency of the apparatus, for a fixed amplitude of 20 mm.

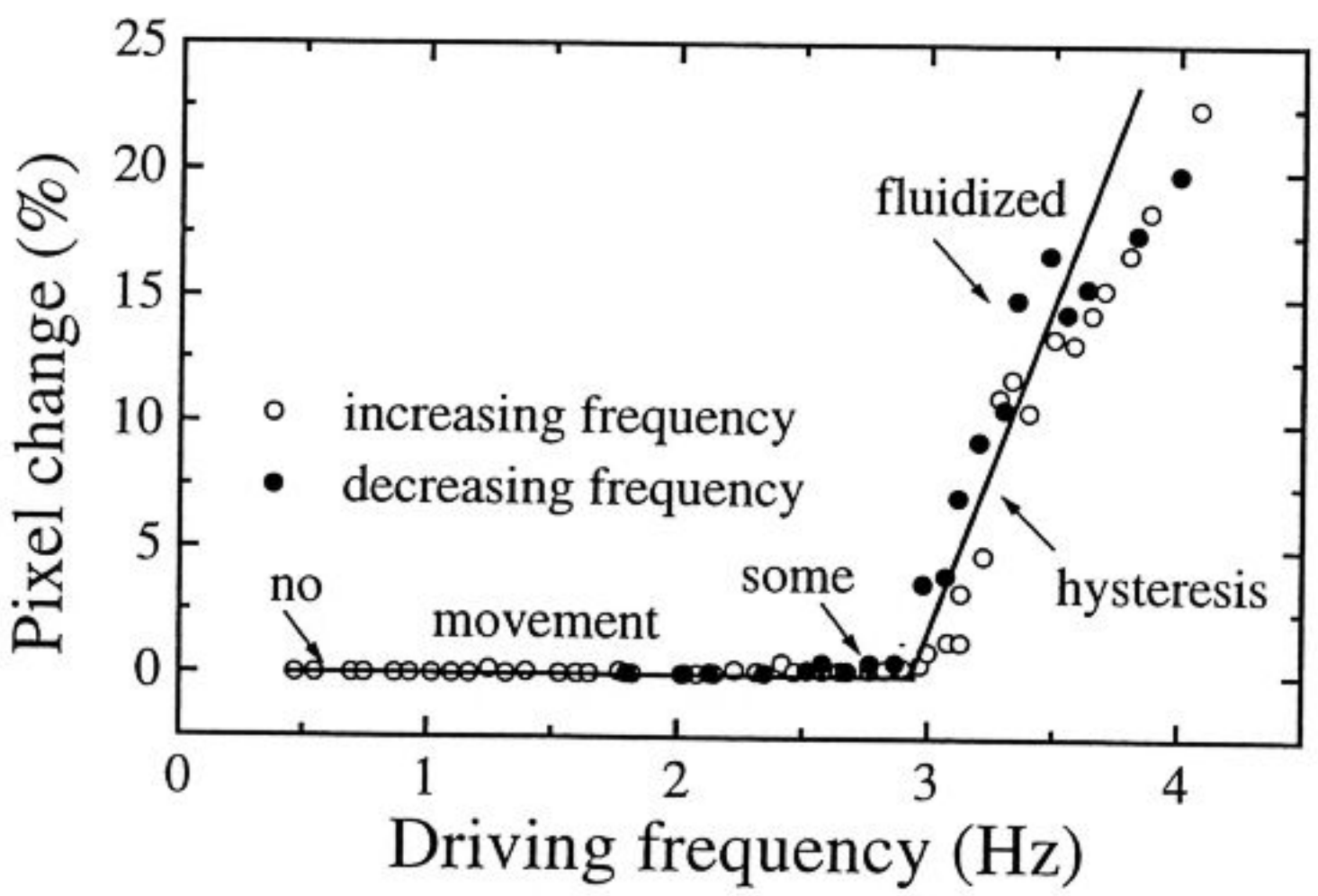


**Fig. 1.** Experimental system: relative pixel change as a function of the external frequency for an amplitude of 2 cm; increasing frequency: ∘, decreasing frequency: •; the solid line is a linear fit to determine the critical point $f_c$.

For low frequencies, the pixel change is zero, indicating that the particles do not move. Above 2.5 Hz the value increases slightly, which we attribute to

the motion of a small fraction of particles. The dramatic increase of the pixel change around 3 Hz defines the transition to the fluidized phase. Open circles are drawn when the frequency is increased between the measurements, and solid circles represent data taken after a decrease of the driving frequency. One can easily distinguish a hysteresis for this transition. We determine the critical frequency $f_c$ for the onset of fluidization by fitting a straight line to the supercritical values. Its intersection with the frequency axis yields $f_c = 2.9$ Hz. The onset of the motion of individual particles, denoted $f_0$, is clearly below this frequency (see Fig. 7 below).

In the second method a laser doppler velocimeter (Polytec LDV-380) was used to measure the particle velocity and the velocity distribution parallel to the direction of the vibration. These measurements served to verify the results obtained by image processing. The measurements were performed near the moment of maximal acceleration of the channel. We compare then the results with those determined by measuring the velocity of a layer of granulate glued in the channel (i. e.w̃ith the velocity distribution caused by finite measuring time and errors in the system). In Fig. 2 the variance of the velocity distribution is shown as a function of the driving frequency of the apparatus. The increase of the variance around 3 Hz is caused by the fluidization of the granulate. This frequency is in good agreement with the one determined by image processing (Fig. 1). The velocity distribution function itself is asymmetric. For frequencies above the transition point there are particles with velocities directed opposite to the driving.

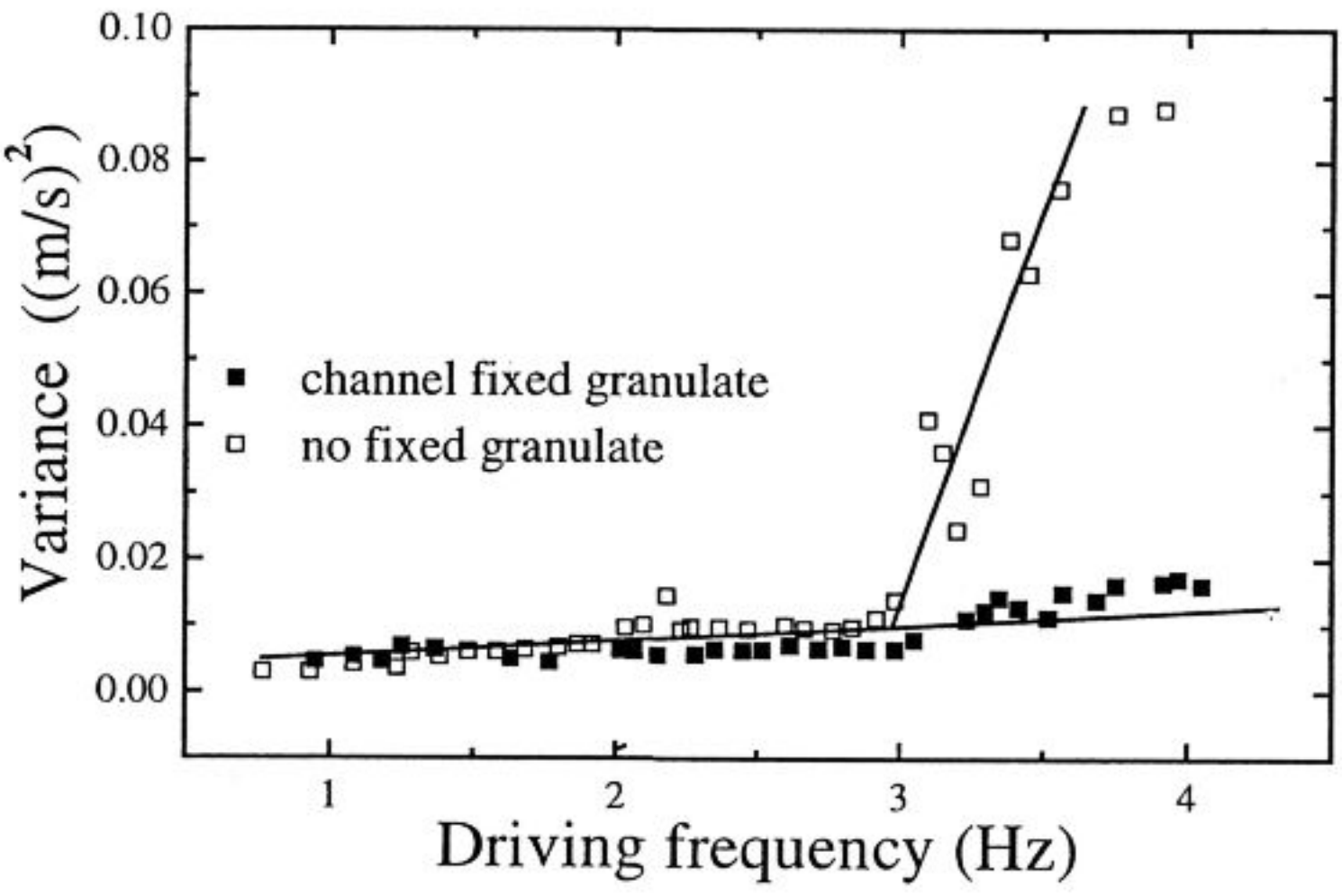


**Fig. 2.** Experimental system: variance of the velocity distribution function as a function of the frequency of vibration for an amplitude of 2 cm.

In order to study granular materials by computer simulations in two di-

mensions, we represent each particle $i$ by a sphere with diameter $d_i$. Only contact forces during collisions are considered and particles are allowed to rotate. We use granular dynamics with a linear springdashpot model and only dynamic friction. The details of the numerical schemes are given in the appendix. In these simulations we have used a value of $\gamma_s = 1$ N s/m, which is sufficiently high so that the shear forces are dependent on $\mu$ only, and $k_n$ was set to $10^6$ N/m. The rest of the parameters were chosen from the detailed collision experiments using glass beads by Foerster et al. (1994) as $\gamma_n = 5.75$ N s/m which corresponds to a restitution coefficient of 0.75 in the normal direction and values of $\mu = 0.1$ for particle–particle and $\mu_w = 0.13$ for particle–wall contacts. In our model, we dissipate energy in the shear direction as well, characterized by a restitution coefficient of 0.75. The box length is 10.08 cm with periodic boundary conditions in the direction of shaking (x-direction) and contained 343 particles in two layers. We use a polydisperse diameter distribution ranging uniformly from 0.52 to 0.60 mm which corresponds to the beads used in our experimental system.

It is easier to determine the fluidization point in the numerical simulations, since the position and velocity information of all particles are given at any time. Noting that the pixel changes in Fig. 1 correspond to particles that have moved in the laboratory frame, we took as a quantitative measure for the phase transition in the numerical system the granular temperature, which is proportional to the velocity fluctuations, $T_g \equiv \frac{1}{N}\sum_{i=1}^{N}\frac{m_i}{2}(\mathbf{v}_i - <\mathbf{v}>)^2$ where $<\mathbf{v}> \equiv \frac{1}{N}\sum_{i=1}^{N}\mathbf{v}_i$. It is averaged over an integer number of full cycles of the external excitation frequency and shown in Fig.3 as function of frequency for the same amplitude as used in Fig.1.

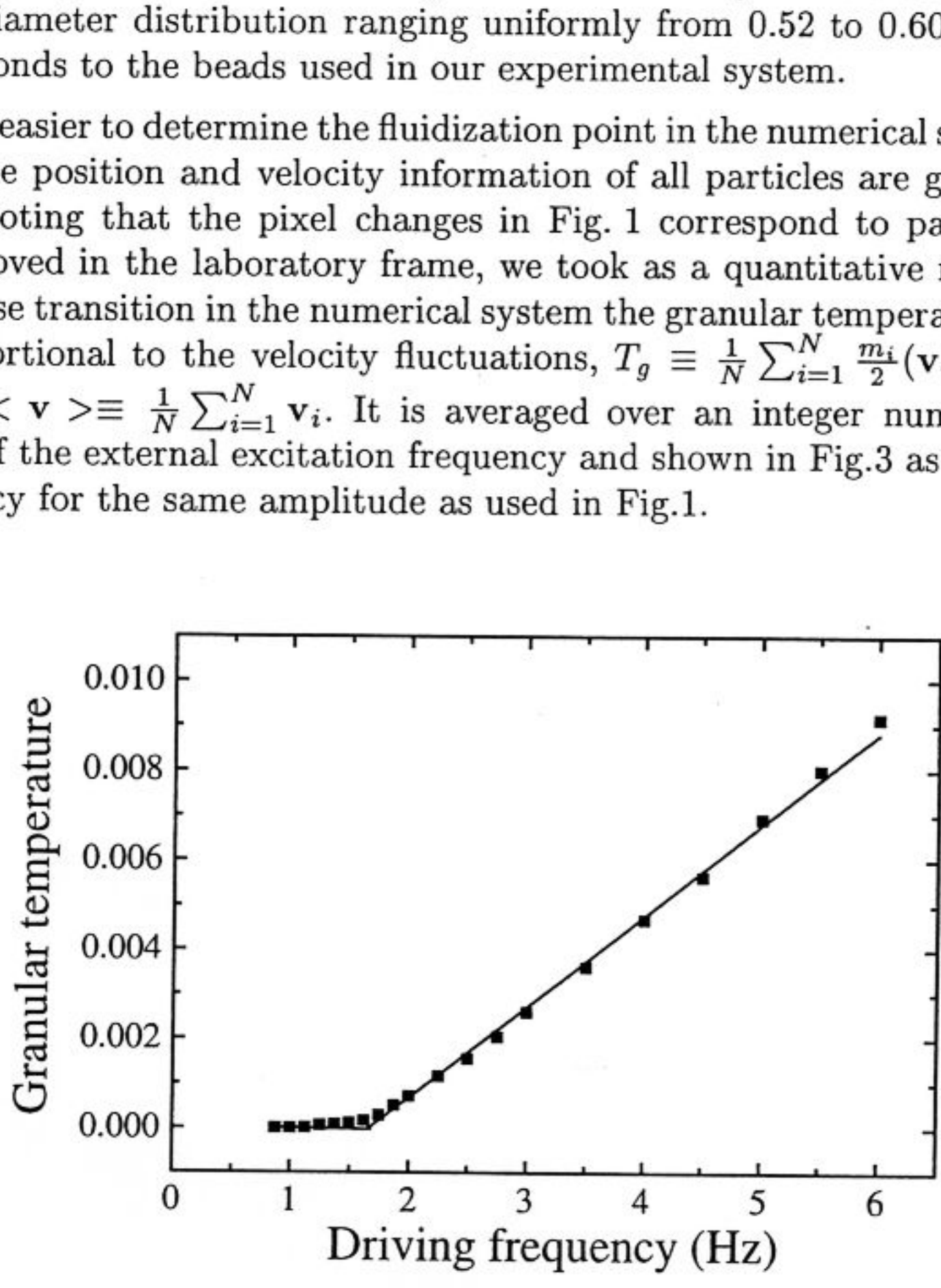


**Fig. 3.** Granular temperature for the numerical system as function of the external frequency for an amplitude of 2 cm.

The error bars are less than the symbol size. $T_g$ is approximately zero for low frequencies and increases monotonically after a transition point which we estimate in a similar procedure as described above as $f^* = 1.7 \pm 0.3$ Hz for $A_0 = 2$ cm. The experimental and numerical system both show the same qualitative behaviour with a well defined transition point. Changing the restitution coefficient in normal direction in the numerical simulations did not change this transition point. On the other hand, changing the Coulomb friction coefficient $\mu$ has a dramatic effect. Setting it to zero lowers the transition point by 0.5 Hz and increasing it to one roughly increases the transition point by 1 Hz as well. We feel that the surface properties of our experimental system does lead to a higher value of $\mu$ than measured by Foerster et al. (1994) which will explain the slight shift. Varying the length of the box size did not change the transition point.

An alternative measure for the transition point can be obtained by looking at the pair distribution function (PDF) defined as (Allen and Tildesley 1990)

$$G(r) \equiv \frac{V}{N^2} < \sum_i \sum_{j \neq i} \delta(|\mathbf{r} - \mathbf{r}_{ij}|) > . \qquad (1)$$

It measures the probability density to find a particle at a distance $r$ from

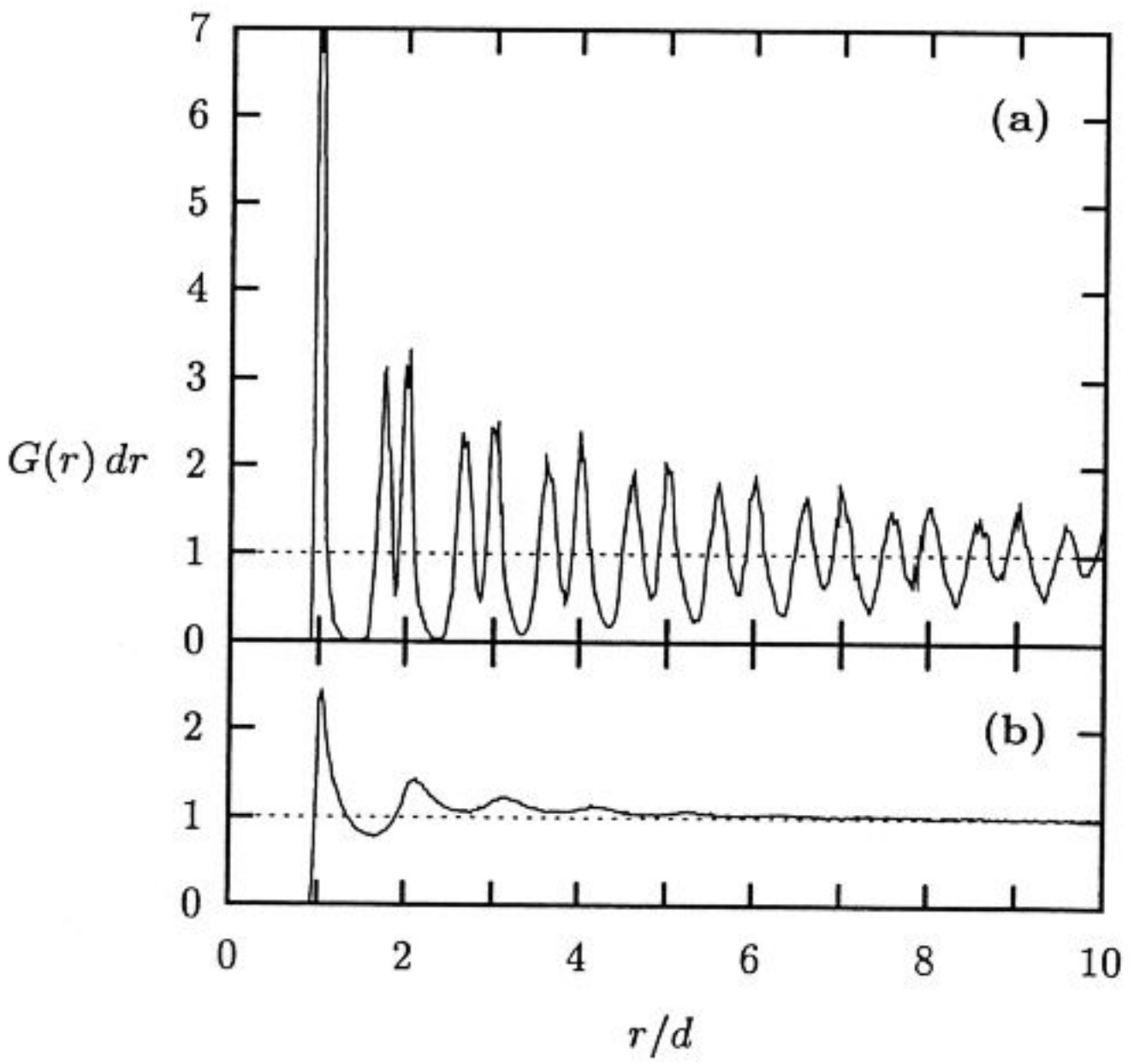


**Fig. 4.** Pair distribution function for the numerical system at a shaking amplitude of 2 cm: (a) at low frequency of 1.25 Hz and (b) at high frequency of 4.25 Hz.

another particle and is normalized to one for a completely random configuration. Clear double peaks are seen around integer values of $r/d$ ($d = 0.56$ mm denotes the average particle diameter) when the system is at rest or only slightly excited, as shown in Fig. 4(a) for $A_0 = 2$ cm and $f = 1.25$ Hz, which is due to the two-dimensional hexagonal packing. Since only two layers of particles are present in our numerical system, we do not distinguish between surface and bulk particles but include all particle pairs in the calculation of the PDF. For the histogram we used a box width of $dr$. The height of the peaks decreases with increasing $r$ because we have a finite system and polydisperse particles. If the external excitation is increased, either by increasing the amplitude or the frequency, the height and the number of clearly visible peaks decreases drastically, as shown in Fig. 4(b) for $f = 4.25$ Hz. This technique was e.g. successfully used to study the melting transition in plasma crystals (Melzer et al. 1996).

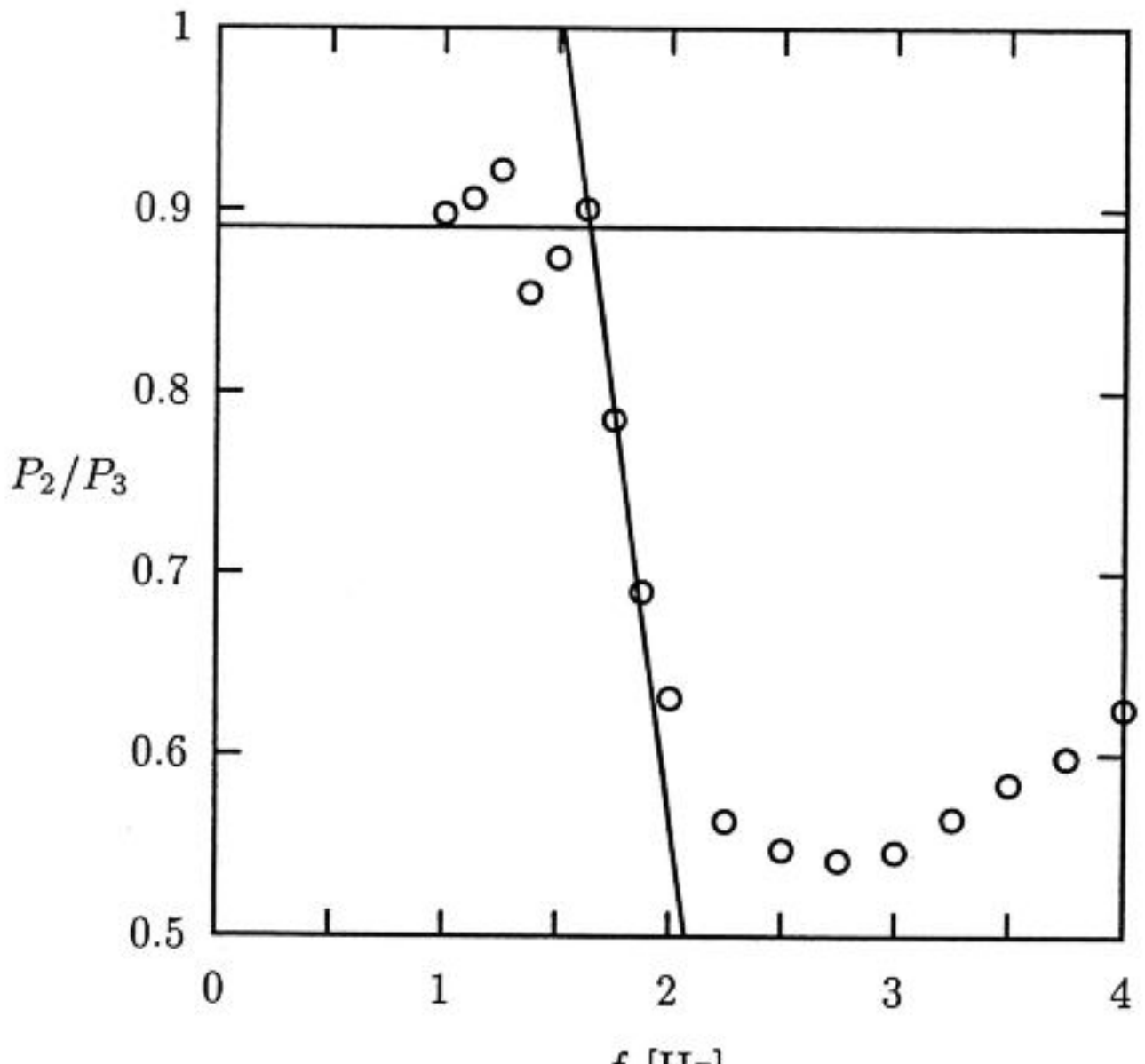


**Fig. 5.** Ratio of the second and third peak of the pair distribution function for the numerical system as function of the external frequency for an amplitude of 2 cm.

In order to quantify the decay of spatial order, we look at the height of the PDF at $r = \sqrt{3}d$ and $r = 2d$, which corresponds to two peaks in the hexagonal packing. The latter corresponds to order within the same particle layer whereas the first measures the order with respect to the neighbouring layer. In an infinite solid phase, both peaks have the same height, whereas the peak around $r \approx \sqrt{3}d$ decreases more rapidly when the excitation is increased and

fluidization sets in, see e.g. Fig. 4(a). We propose as second order parameter the ratio of the heights, measured with respect to the constant background value of one, of these peaks, denoted by $P_2/P_3$. This is illustrated in Fig. 5 for a shaking amplitude of 2 cm. A qualitative change of the curve is seen around $f = 1.6$ Hz when the nearly constant ratio starts to decrease monotonically. This change corresponds to the transition point and its value, given by the intersection of the two straight lines in Fig. 5, is in perfect agreement with the one obtained using the granular temperature.

The increase with frequency of the kinetic energy or of the granular temperature varies much with the excitation amplitude. All curves collapse onto one universal curve when they are plotted as function of the dimensionless parameter $\Gamma \equiv A_0(2\pi f)^2/g$, where $g$ denotes the gravitational constant, and the granular temperature is rescaled with the maximum excitation velocity to the power of 1.66. This might be related to the 5/3 law discussed by Taguchi (1993) and Ichiki and Hayakawa (1995). Here we use dimensionless quantities denoted by the superscript $s$ using the average mass and diameter of a particle and also g, which is shown in Fig. 6 for three different shaking amplitudes. It is reminiscent of the scaling of the center of mass of a granulate under vertical vibration in two dimensional simulations where an exponent of 1.5 has been found (Luding et al. 1994). The error in our exponent is 0.05.

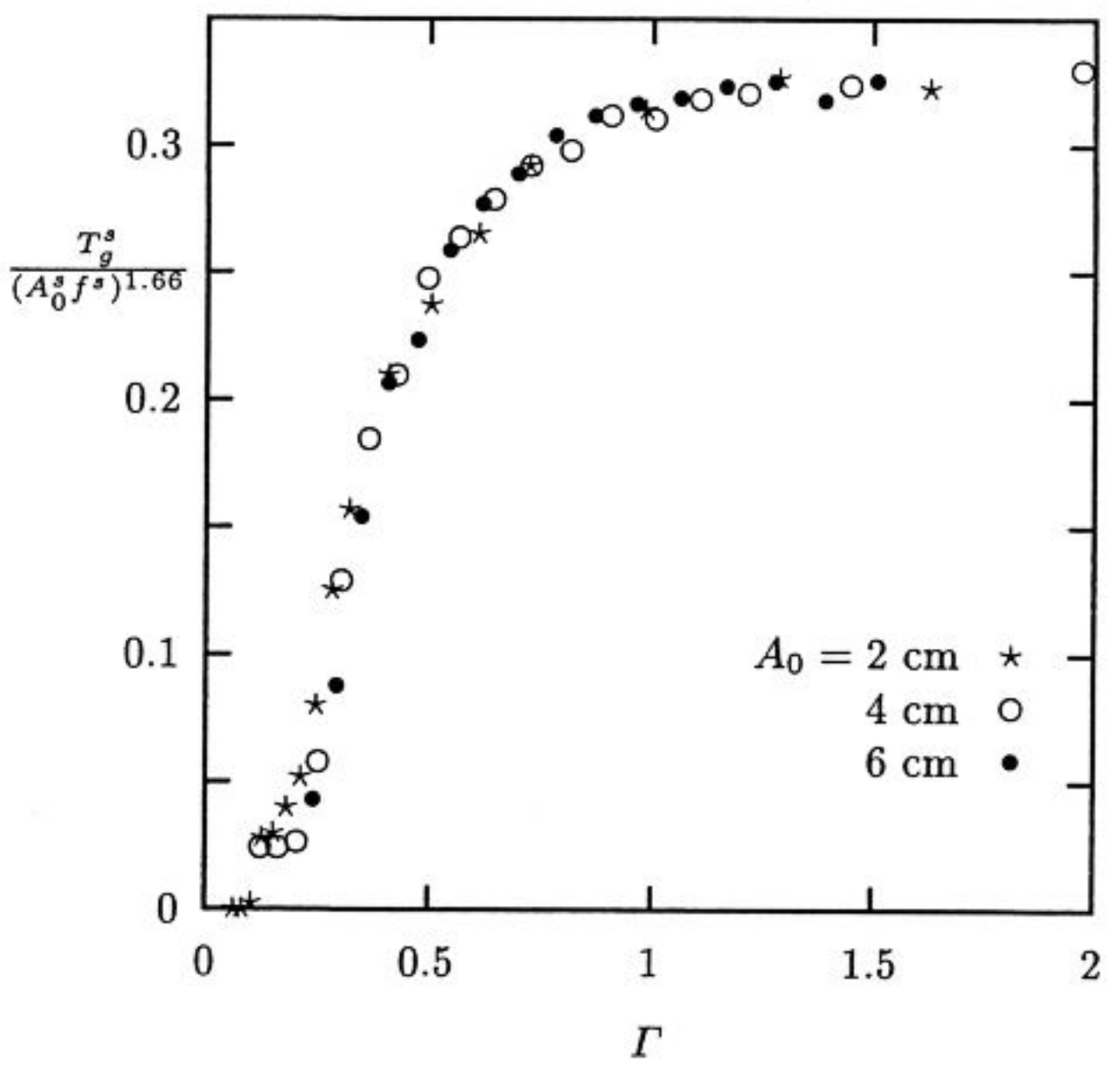


**Fig. 6.** Numerical simulations: rescaling of the granular temperature as function of $\Gamma \equiv A_0(2\pi f)^2/g$.

In order to find the correct scaling parameter for the horizontal shaking experiment, we look at a two-dimensional cross section of the system similar to the one used in the numerical simulation. Since the particles vary in diameter by only ± 7 %, a nearly hexagonal packing is found when the vibrations are switched off, i.e. one cylinder in the upper layer rests on two cylinders from the next layer below. For an estimate of the solid–fluid transition, one can then calculate the critical acceleration where a single cylinder would begin to move within the valley formed by these two cylinders to be $a_c = g \tan 30°$. This yields the following scaling of the critical frequency with the amplitude: $f_c \sim \sqrt{g/A_0}$.

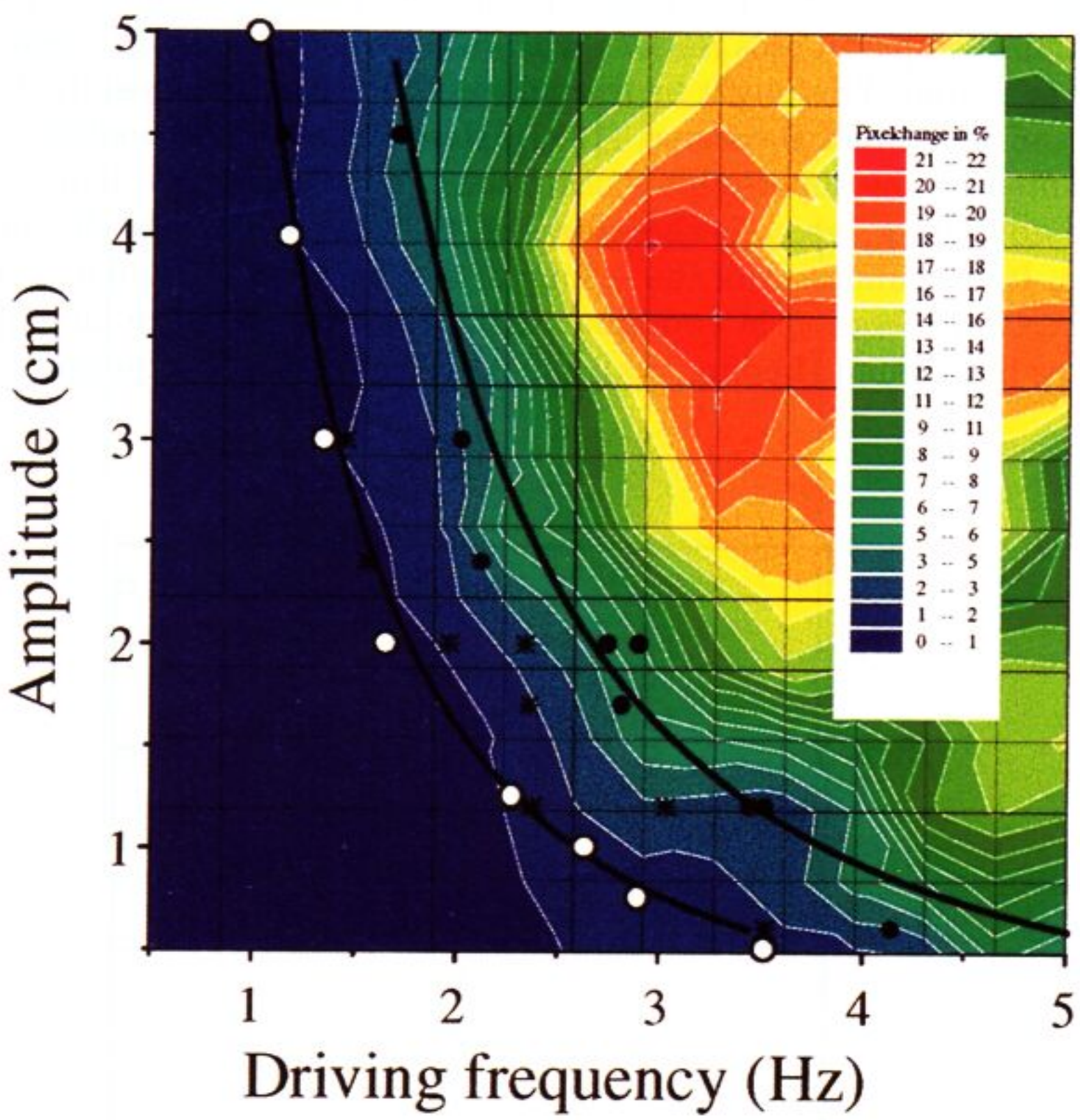


**Fig. 7.** Phase diagram for the solid–fluid transition: experimental points ⋆ ($f_0$) and • ($f_c$) with color scale image of the pixel change (see legend); data from numerical simulations ∘ with thick solid line as best fit. The thin solid line shows the theoretical curve.

Fig. 7 summarizes the results of the experimental, theoretical and numerical estimates for the solid–fluid transition. In order to avoid the ambiguity caused by the rounded transition from a solid to a fluid like state, we present

the amount of the pixel using a color scale. The transition from no movement to a 1% change corresponds to the transition denoted $f_0$ above. It seems to agree fairly well with the analytical argument and with the results of the molecular dynamics simulation. The experimentally determined solid–fluid transition, denoted $f_c$, is obtained at slightly larger values of the driving acceleration. The difference between theory and experiment might be due to the additional friction caused by the side walls in the experimental setup.

## 3.2 Segregation of Granular Materials

One of the most puzzling phenomena encountered in granular matter is segregation of a polydisperse mixture of particles. In spite of much work, relatively little is known about the basic physical processes involved in the dynamics of the segregation of granular media and many puzzles remain to be solved in this field. Apart from posing numerous fundamental and difficult questions from a theoretical point of view, knowledge of segregation is needed for many industrial applications. The segregation of particles with different properties is a ubiquitous process of major importance in areas as agriculture, geophysics, material science, and almost all areas of engineering, i.e. involving preparation of food, drugs, detergents, cosmetics, and ceramics. Segregation also appears during industrial processes such as drying and coating of granular material in rotating kilns.

A common feature of all these processes is the dynamical interplay of polydisperse granular particles. Segregation can be brought about by many processes including pouring, shaking, vibration, shear and fluidization. For such systems the random mixed state is not stable and the different particle types tend to separate. In most cases the particle size is by far the most important property controlling segregation and size segregation is observed even in processes designed for particle mixing (Donald and Roseman 1962, Williams 1976, Bridgewater 1976). However, all these articles describe mechanisms for the phenomena rather than an explanation of the effects; i.e. they tell us how the particles move and not why. Size segregation seems to contradict equilibrium statistical mechanics since the density of the overall packing decreases with the amount of segregation, i.e. entropy is reduced by segregation. Segregation can occur whenever a mixture of particles of different sizes is disturbed in such a way that a rearrangement of the particles occurs; i.e. the mixture gets fluidized or expanded. There gaps between particles will occur, allowing a small particle to traverse through whereas for large particles the gaps are too narrow.

**Segregation Driven by Vertical Vibration.** A common way to achieve segregation is shaking in vertical direction, where one can observe the so called "Muesli effect". When a box of muesli is shaken, the large nuts and raisins are moving to the top of the muesli and do not get mixed. In general,

a large ball placed at the bottom of a vibrated bed will rise to the surface. This effect occurs even if the large particle is denser than the fine particles. Two main driving mechanisms have been proposed.

One, for low accelerations is that the granular material becomes dilated with free volume introduced during each shaking cycle. The smaller particles fall relatively free; while the larger particle are prevented from doing so by statistical unlikelihood of collective motion forming such voids. Therefore the large particle rises and segregates. In this regime, segregation is interpreted as the result of competition between independent particle dynamics and collective reorganizations (Williams 1976, Dippel and Luding 1995).

The other mechanism, preferably for high accelerations, is the formation of bulk convective flow of the bed particles which, at the same time, carry the intruder (Knight et al. 1993, Cooke et al., 1996). When the large particle reaches the top, it is not able to penetrate the top layer to move downwards with the flow and therefore stays at the top. Boundaries play a crucial role in initiating and sustaining the convective flow. In this regard, these materials behave very differently from ordinary fluids where buoyancy forces can drive convection. Convection appears to be directly linked to the interaction of the beads with the container wall, i.e. higher wall friction increases convection.

However, in both cases, the size ratio and the time dependence of the phenomenon is not quite understood. In general, the speed of the segregation is profoundly dependent upon the vibration frequency. For each system there is an optimum frequency for the segregation process, but this frequency varies from system to system. This is still an unsolved problem and the dependence of the segregation on the frequency is yet not fully understood (Vanel et al. 1997).

**Segregation Driven by Horizontal Vibration.** A relatively unexplored question is the behaviour of particles that are subject to horizontal shaking. During vibration in horizontal direction convective motion on the surface can be observed. This can give rise to a "reverse Muesli effect", where the large particles, initially, move towards the bottom of the particle bed (Liffman et al. 1997). In fact, horizontal shaking can produce two sets of convection cells in a box of granular material. The upper set of convection cells arises due to surface-wave effects, with material convecting up the side walls and down at the center of the heap. The lower convection cells move in opposite direction, i.e., down the side walls and up in the middle of the box. They arise due to the, gravity induced, downward movement of particles in the intermittent gaps that form between the heap and the side walls.

This convective behaviour give rise to a "reverse Muesli effect", where a large particle placed at the top-center of the pile will convect downwards until it reaches the upwelling of the lower convection rolls. For "small" heaps, the large particle will actually reach the bottom. In both cases, the surface-wave convection may cause a "large" particle to return to the top of the pile.

**Stratification (Segregation by Pouring).** Segregation also occurs when a mixture of particles is poured onto a horizontal plate. A spontaneous stratification appears, with alternating layers of small and large particles parallel to the surface of the sand pile. Whether this stratification appears only in two dimensions (Makse et al. 1997) or also in three dimension (Julien et al. 1997) still needs to be clarified. This mechanism could play a paramount role in the formation of thick stratified sediment deposits, which can be seen nowadays in sand stone rocks. Additionally, there is an overall tendency for the large and small particle to segregate spontaneously in different regions of the heap.

**Hopper.** In conical hoppers, most of the segregation occurs during the filling process through flow at the free surface when particles are poured into the hopper from the top. Small particles will accumulate in the central region whereas larger particles can mostly be found close to the side walls due to their higher mobility (Brown 1939, Standish 1985).

Two basic types of motion can be distinguished in hopper: (i) funnel–flow behaviour where the flow mostly occurs in a central region which might lead to the formation of rat holes (Johanson 1978) and (ii) mass-flow behaviour where flow occurs everywhere in the bin which can lead to *first-in-first-out* characteristics (Jenike 1964). The latter operational mode can also lead to a re-mixing of particles and thus reduce segregation.

**Radial Segregation in a Horizontal Rotating Drum.** Radial segregation in rotating drums takes place on very short time scales (Donald and Roseman 1962). Usually the drum is roughly about half-filled and rotated along the cylinder axis about the horizontal (see Fig.8). When the drum rotates, most particles can be viewed as being part of a solid block rotating upwards. On top of it, a fluidized layer is formed with downward flowing particles. For a small angular velocity, $\omega$, there are distinct avalanches which are well separated. For increasing angular velocity, the avalanches follow each other more rapidly and finally exhibit a continuous downwards flow for a particular range of the angular velocity $\omega$. For even higher speeds, the particles are centrifuged to the drum wall, but no segregation is observed in this regime. The kinematics of the segregation happens only in the shear flow along the surface, in that the small particles percolate between the larger ones in the flow and get trapped by the solid block before they can reach the cylinder wall. Due to the continuous solid block rotation, a core of small particles at the center of the drum below the surface flow is formed. This is commonly referred to as *radial segregation.* In two-dimensional systems, this was well observed experimentally (Clément et al. 1995, Cantelaube and Bideau 1995). Using discrete element simulation one can define an order parameter, $q$, that allows to quantify the amount of segregation. It can be used to compare the segregation speed and the final amount of segregation, $q_\infty$, for different systems and materials directly (Dury and Ristow 1997). The width

of the fluidized layer plays an important role and it is found that with increasing width, $q_\infty$ will decrease since more and more portions of the already segregated regions will be destroyed again. The segregation speed also increases with the rotation speed of the drum which corresponds to an increase in width of the fluidized layer as well.

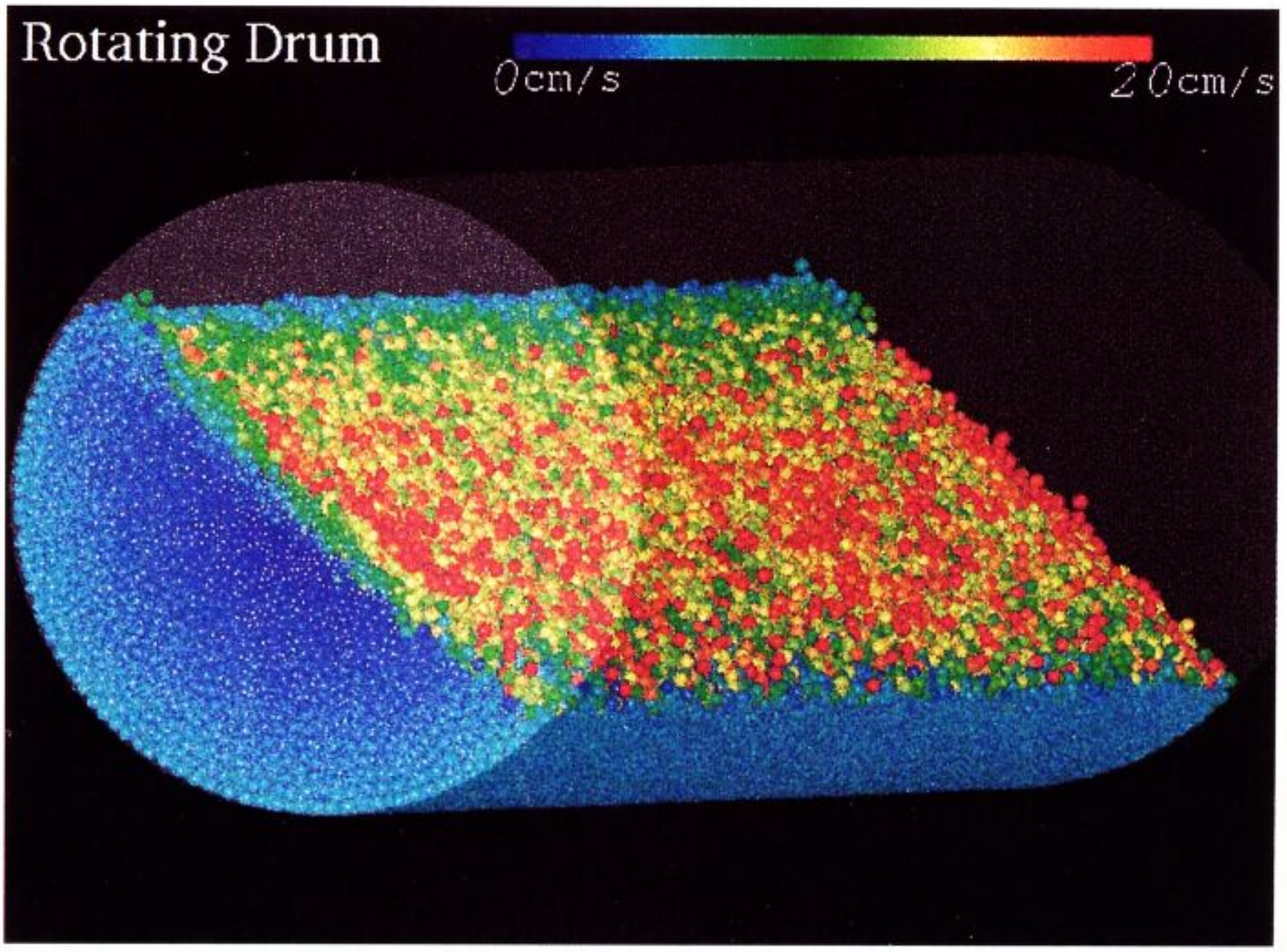


**Fig. 8.** Picture of the drum looking from the side. The particle velocities are color coded.

However in three spatial dimensions, radial segregation is more easily to achieve, since the voids between the particles are connected by a network and small particles can traverse more easily through it than the large particles, which will lead to a better segregation. Also in three dimensions, small particles colliding with larger ones can be deflected parallel to the direction of the rotational axis and therefore the velocity in direction of the downwards flow is reduced. Hence the particles have more time to segregate until they hit the wall (Dury and Ristow 1997). To verify this, an extended three-dimensional drum was simulated, containing a binary mixture of a total of more then 280 000 of small and large particles having a size ratio of 1.65:1, and a number ratio of 1:1, see Fig. 8. In Fig. 9, the segregation parameter is shown as a function of the drum rotations for two different widths of the fluidized layer. The upper curve corresponds to a narrow layer and shows a very fast

segregation whereas the lower curve corresponds to a much wider layer and shows a significantly reduced segregation speed. A clear saturation is not yet visible but by inspecting a cross-section for the fast segregating system after two drum rotations, shown in Fig. 10, a nearly complete radial segregation of the smaller dark particles to the center is clearly visible. These preliminary results indicate that our hypothesis about the influence of the dimensionality on the segregation speed seems justified but for a more conclusive judgment, we have to rotate longer and wait for a saturation of the order parameter $q$.

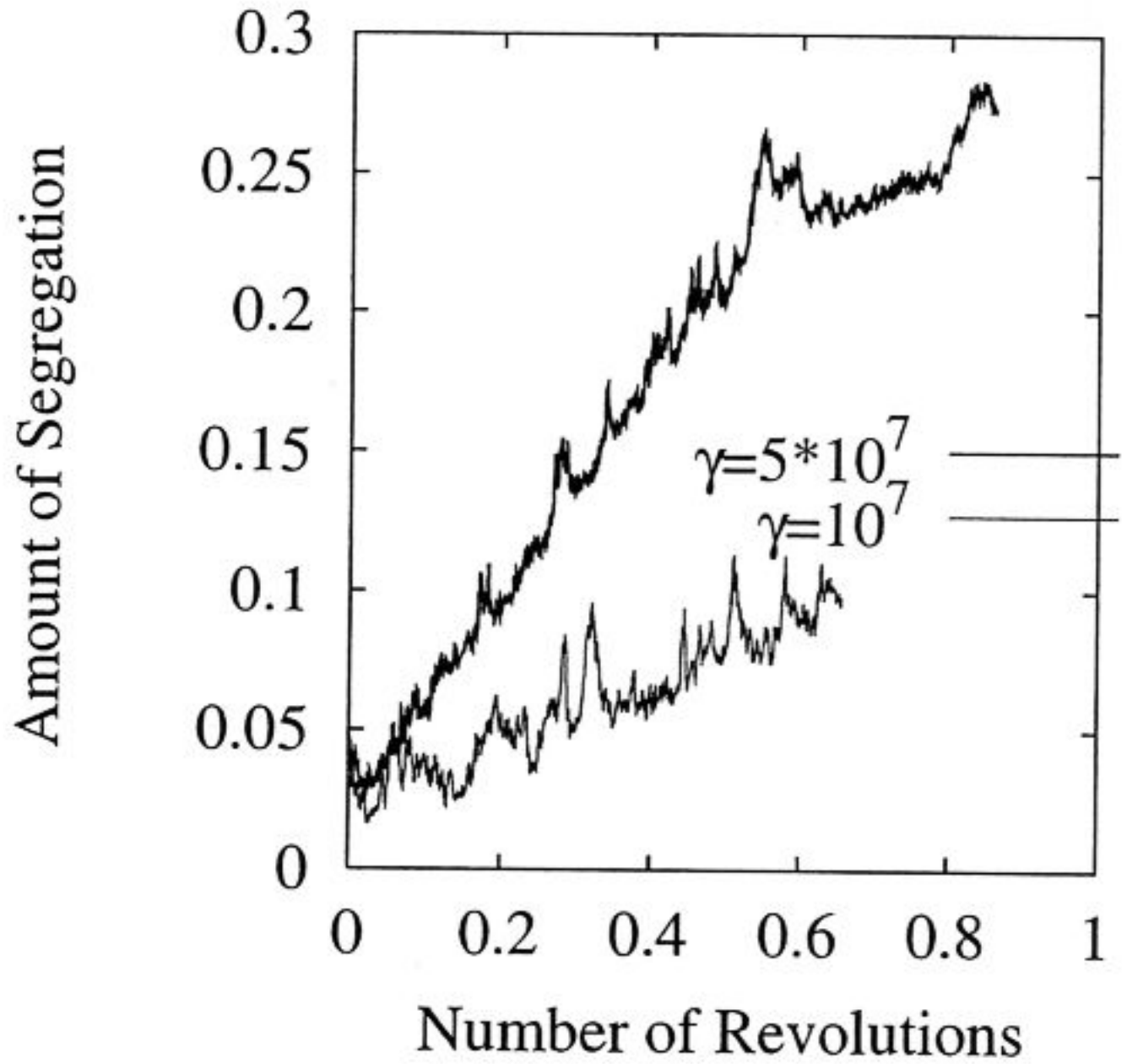


**Fig. 9.** Time evolution of the segregation order parameter for two different widths of the fluidized layer; narrow: upper curve, wide: lower curve.

Another point which has been observed is, that depending on the filling fraction there is also geometrical mixing (Metcalfe et al. 1995) which competes with the radial segregation. For a half-filled drum, mixing is minimal and segregation should therefore be maximal, whereas for a roughly quarter-filled drum, mixing is maximal and therefore segregation should be less pronounced than in the half-filled case. This interplay of mixing and segregation was recently studied numerically (Dury and Ristow 1998). It was found that the fastest and most complete segregation is achieved for a filling fraction of about 60% rather than the predicted 50%. This difference can be explained by the width of the fluidized layer since the numerical work was done in the continous flow regime.

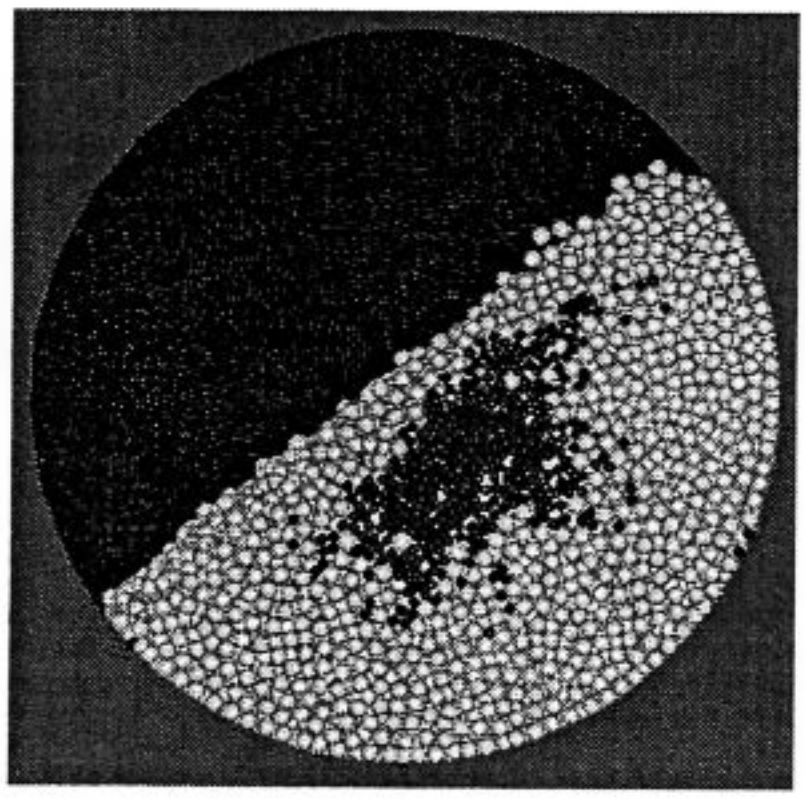

**Fig. 10.** Snapshot after two rotations for the faster segregating system leading to a concentration of small particles in the central region.

**Axial Segregation in a Horizontal Rotating Drum.** On the other hand, axial segregation happens on a much longer time scale than radial segregation. Axial bands are typically formed within minutes to hours. Also in contrast to the radial segregation, not all polydisperse systems show axial segregation; it is still an unsolved question whether a polydisperse mixture of particles will eventually segregate or not. The phenomenon of axial segregation has been long known (Donald and Roseman 1962) and an example is shown in Fig. 11. But the origin of the bands (Nakagawa 1994, Zik et al. 1994, Hill and Kakalios 1995) and whether they are stable or not (Choo et al. 1997) is still debated.

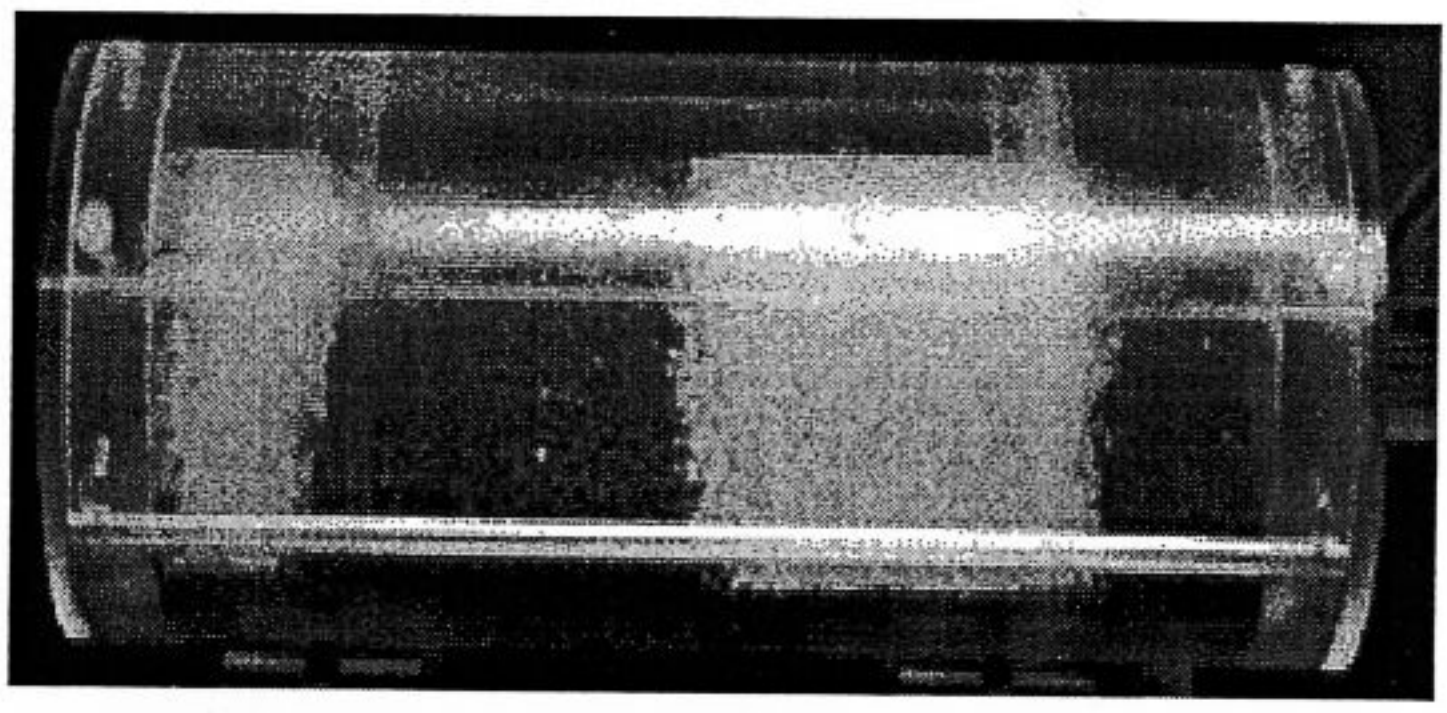

**Fig. 11.** Photo of a 50:50 volume mixture of poppy and mustard seeds after rotating for 1 hour at 30 rpm. A nearly perfect axial pattern is clearly visible.

One suggested mechanism builds on the observation that axial segregation occurs when the smaller particles have a higher angle of repose (the angle of repose is the angle between the horizontal and the surface of the granular mixture, Das Gupta et al. 1991). Due to local concentration fluctuations there will be regions with less small particles and therefore with a lower angle of repose. Now the larger particles from the neighboring sides with the higher angle of repose will go into this region and therefore enlarge the fluctuation. This systematic self-concentrating effect leads to zones with no large particles and zones with a very high percentage, eventually 100%, of large particles. Another possible mechanism is due to the percolation of small particles in the solid block. This might become the dominating mechanism when the radial segregation has set in. In that case, only few small particles will be present in the fluidized surface layer and the particle transport of the smaller species has to go through the radially segregated core. But more work needs to be done to fully understand the interplay of these mechanisms.

In order to investigate the band formation, we prepared different binary mixtures, 50:50 by volume, of various round particles, e.g. glass beads, pharmaceutical pills, mustard and poppy seeds. No band formation could be observed using the pharmaceutical pills and the most stable configuration was obtained by using small mustard seeds with a diameter of 1.7 mm and poppy seeds with a diameter of 1 mm. The drum was 26 cm long, 7 cm in diameter and half-filled with the initially well mixed particles. In Fig. 12, we show the concentration of poppy seeds along the rotation axis in weight percentage.

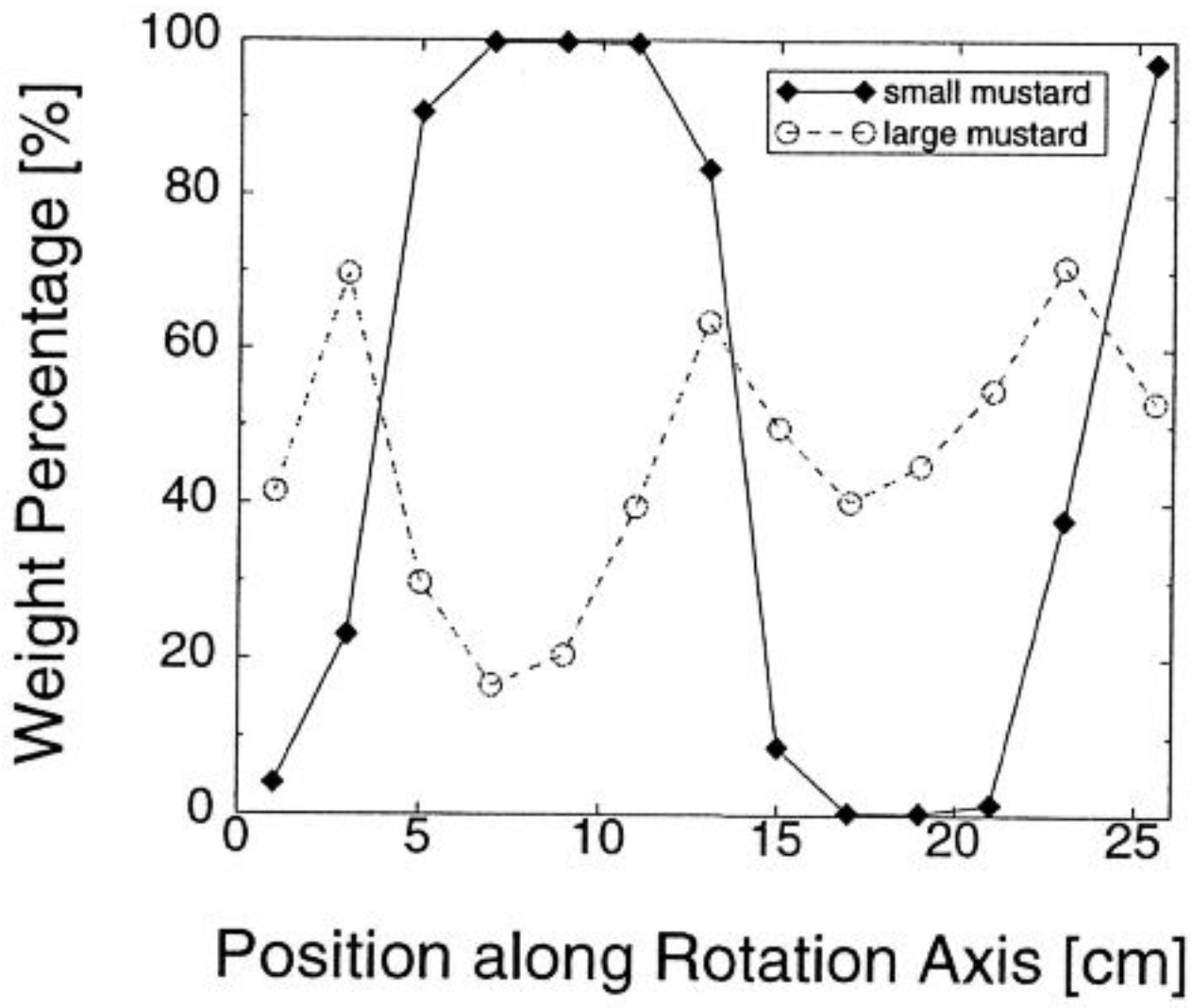


**Fig. 12.** Weight percentage of poppy seeds in a 50:50 mixture by volume with mustard seeds of different sizes. Axial bands are much more pronounced for small mustard seeds.

Two curves are shown: Filled diamonds correspond to the small mustard seeds and give an average value of 49.7%, whereas the open circles correspond to the of slightly heavier larger mustard seeds with a diameter of 2.5 mm and an corresponding average value of 45.7%. For this experiment the drum was rotated for one hour at 30 rpm and the mixture of small mustard seeds with poppy seeds shows a very sharp and pure stable 4 band pattern. The mixture of large mustard seeds with poppy seeds did not show very pure bands, i.e. the concentration is not close to 0 or 100%, the number of bands is between 5 and 6, and was not as stable as the previous combination of the mixture.

## Ripple Formation Induced by Water Shear Flow

One of the most obvious examples of pattern–forming systems in nature are the ripples and dunes formed in sand, either by the wind, by steady (i. e. rivers) or oscillatory flow (i. e. surface waves). Apart from the basic instability triggering the ripple formation the dynamic behaviour such as the travel velocity of the established ripples is not understood.

In order to investigate this transition we have designed an annular shaped channel which is sketched in Fig. 13. The annular channel has an inner diameter of 292 mm and a channel width of 46 mm. The thickness of the inner and outer cylinder made of Perspex (Röhm) forming the annular channel is 4 mm. The channel is 60 mm high and is filled with glass beads of $150-250\mu$m diameter. The distance between the sand surface and the rotor disk, later referred to as $h$, is $18-21$ mm. The channel walls are made of Perspex and fixed on a plate of aluminium. This arrangement is placed in an aquarium filled with water up to 10 cm above the upper edge of the channel. The experiment were performed at room temperature. Above the channel there is a rotor dish of $D_r = 290$mm diameter made of Perspex which is connected to a motor and gear unit (Mattke Antriebstechnik). The rotor disk reaches 4 mm into the channel. The reducing gear (Stöber) with a reduction of 10.3 is used to have the motor run in the area of smallest wow and flutter. The frequency of rotation of the motor is set by a controlling unit which is driven via the serial interface by a PC (90 MHz Pentium). The variations of the frequency of rotation is less than 0.1% according to the manufacturer. A CCD–camera (Sony) fixed in the laboratory frame and controlled by a frame grabber card (Leutronvision) is observing a window of 100 mm in width and a height capable of covering the interface curve between the sand and the water flowing above it. With a constant sampling rate $f_s = \frac{1}{T}$, the boundary between sand and water is detected with the help of the gradient in contrast between the bright sand and the darker water. The parametrized boundary is stored for the purpose of further evaluation.

In Fig. 14 the dependence of the amplitude, the velocity and the total number of the ripples on the Reynolds number is given. In order to obtain these data all measurements were performed with a flat sand surface and zero rotation of the rotor disk as starting conditions. The rotor is speeded up

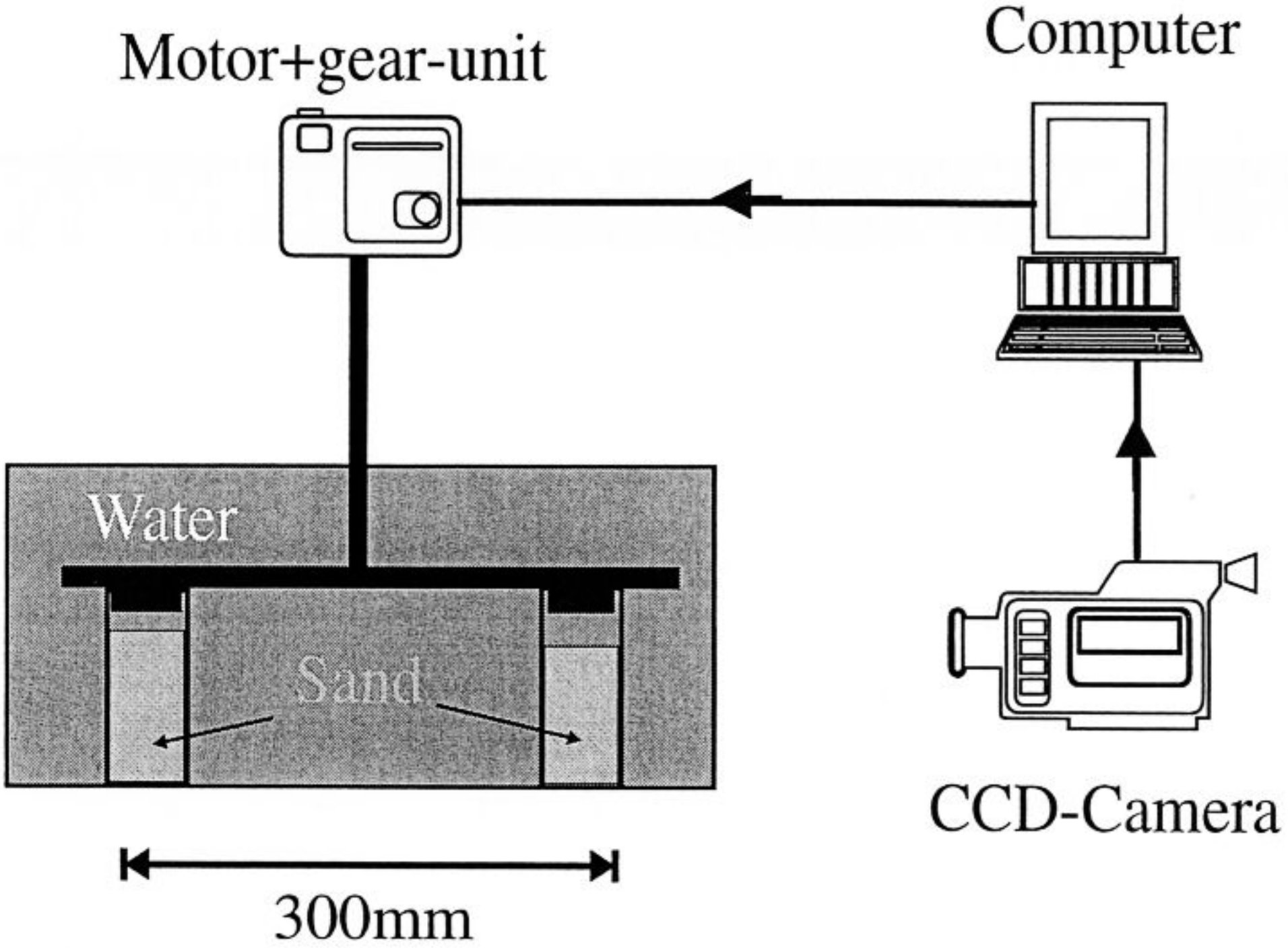


**Fig. 13.** Experimental setup for water shear flow.

within a few seconds to a certain frequency. This frequency corresponds to the Reynolds number on the abscissa of Fig. 14 via $Re = \frac{\rho u h}{\mu}$. Here, $u$ denotes the maximal azimuthal velocity $u = \pi f D_r$ of the rotor disk of diameter $D_r$ rotating at the frequency $f$ and $h$ is the distance between the flat sand surface and the rotor disk. The values for the density $\rho$ and the viscosity $\mu$ of water are taken at room temperature. For each Reynolds number we wait for a time $t_w$ of half a day before starting the data acquisition. The amplitude, which is plotted in the lower part, is determined by the difference between the maximal and the minimal amplitude of a ripple $(A_{max} - A_{min})/2$. For each Reynolds number this procedure is repeated at least 100 times. The error bars are given by the standard deviation $\sigma = \frac{1}{N}\sum_{i=1}^{N}(A_i - \bar{A})^2$. The solid line is a fit of a square root function (expected for a supercritical bifurcation) to the lower eight data points. The travel velocity of the ripples shown in the middle part of Fig. 14 was determined from the shift L of two consecutive boundary curves via a correlation function. As the sample time between two consecutive data sets is T, one can calculate the travel velocity $v = \frac{L}{T}$. Again the error bars give the standard deviation. In the upper part of Fig. 14 the

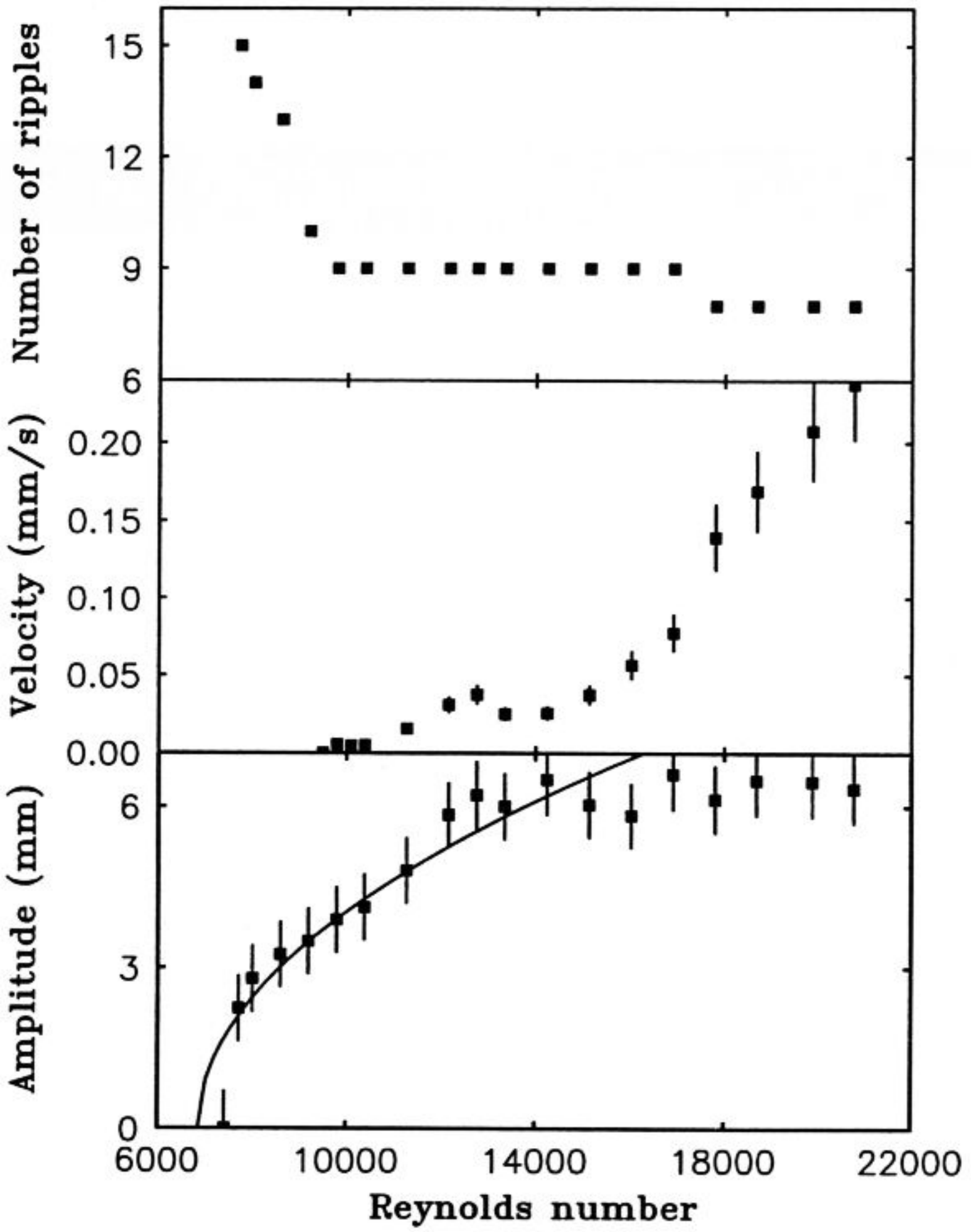


**Fig. 14.** The dependence of the amplitude (lower part), the velocity (in the middle) and the number of ripples (upper part) on the Reynolds number.

number of ripples along the circumference of the channel after running the experiment with a fixed frequency of rotation for time $t_w$ is shown. This quantity was determined by visual inspection.

On the basis of Fig. 14 we interpret the transition from the initially flat to the rippled sand surface as a supercritical bifurcation taking place at a Reynolds number of 6860. We have not been able so far to measure the details of the transition because the time necessary to establish ripples all over

the circumference increases rapidly as the critical Reynolds number is approached. In this regime no velocity data are available because the possibly very small movement is beyond our experimental resolution. A clearly measurable velocity sets in at a Reynols number of about 9500. This increase of the speed is accompanied by a dramatic change in the slope in the upper curve. We cannot offer an explanation for this observation. The second transition takes place at a Reynolds number of about 14000, where again a qualitative change in the velocity occurs and the amplitude saturates.

All three observations need to be investigated in more detail. Our current work focusses on the transition from a flat sand surface to a ripple pattern, however.

## Pattern Formation under the Influence of Horizontal Vibration

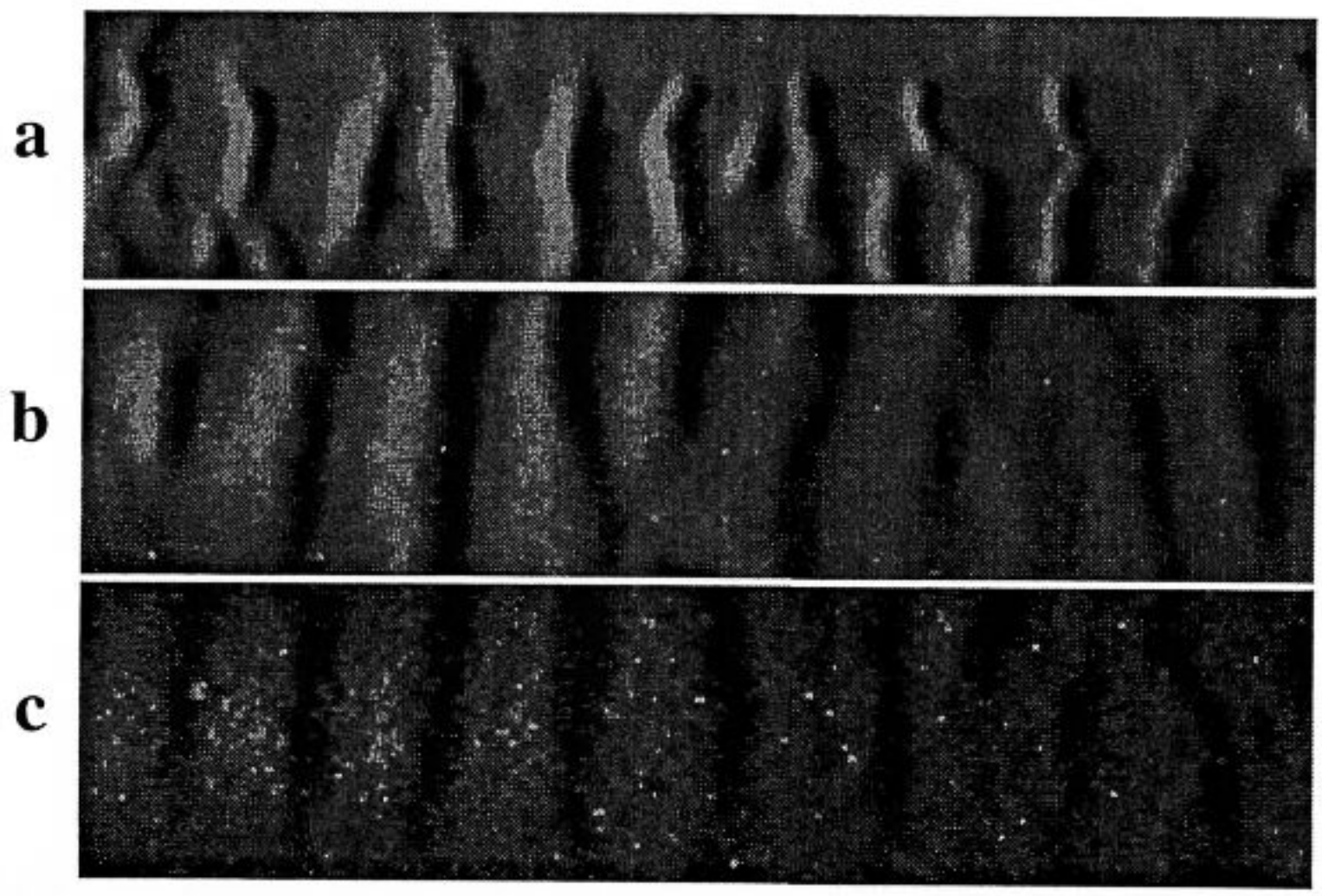


**Fig. 15.** Patterns generated during horizontal vibration. Dumping height between one and three layers of granulate, 25 cm of a channel with a total length of 35 cm are visible, driving amplitude: 2 cm, driving frequency: 4 Hz, material: glass spheres with different diameters: a) $150\mu m \leq D \leq 160\mu m$, b) $210\mu m \leq D \leq 250\mu m$, c) $430\mu m \leq D \leq 600\mu m$.

The behaviour of granular matter under the influence of periodic forces has so far mostly been studied on systems which are vibrating parallel to the gravitation field (Melo et al. 1994, Jaeger et al. 1994, Luding et al. 1994). Only a few works focus on horizontal driven systems. Evesque (1992) and

Rosenkranz and Pöschel (1997) reported about an experiment with horizontal vibrated granular matter and large dumping heights. Above a given threshold of vibrating amplitude they observed a small convexity of the free surface of the pile and a convection flow.

We are dealing with the behaviour of only a few layers of granulate after fluidization. For a pattern formation under horizontal vibration, which is stable in space and time, one can use vibrating plates or channels. In Fig. 15 some images of patterns are shown. There are many parameters which may influence the pattern, e.g. the properties of the granulate, the roughness of the container surface, the driving amplitude and frequency. The influence of some of these parameters on the pattern formation have been studied qualitatively. We find that already a monolayer or even less than a monolayer of granulate is sufficient for cluster formation. For a characterisation of the density of the granulate in such a system we use the "solid fraction" (McNamara and Young 1996). Because of the relatively small number of particles that exist in such a system it could be simulated numerically by means of molecular dynamics. A theoretical description with similar approaches as used by Sela et al. (1996), McNamara and Young (1996), Spahn et al. (1997), and Grossmann et al. (1997) seems to be possible.

For generating the vibration and capturing the pictures we used the setup described in section 3.1. As container for the granulate we used boxes at 4 cm width and with a length between 35 and 47 cm in the direction of vibration. The container was made of aluminium and had a plastic foil with a roughness of 7 $\mu$m glued on its bottom. A CCD–camera observed the container from above, i.e. perpendicular to the direction of vibration. We used grazing incidence of parallel light along the direction of the oscillatory motion to visualise the modulation of the surface. When using less than one monolayer of granulate we illuminate with divergent light from a point source, which is perpendicular to the channel, to visualize the fluctuation of the grain density. For the determination of space–time–diagrams we measure the intensity along one or more lines of a frame. The measurement can be taken at any stage of the motion. For time–resolved measurements of cluster formation and cluster interaction a high–speed–camera (1000 frame/s, 5400 frames) was used. The material used in preliminary measurements was the same as in section 3.1. Later we used real granulate (grains of seed) and monodisperse steel spheres with polished surface.

**Influence of the Channel Walls on the Patterns.** The influence of the channel walls can be seen in Fig. 16. The wavelength seems to rise with the channel width. The channel with the largest width has a wavelength close to the one formed in a layer that has no contact with the boundaries at all. This channel width was used in the following experiments, i.e. the influence of the channel walls parallel to the direction of vibration has only little influence in our experiments.

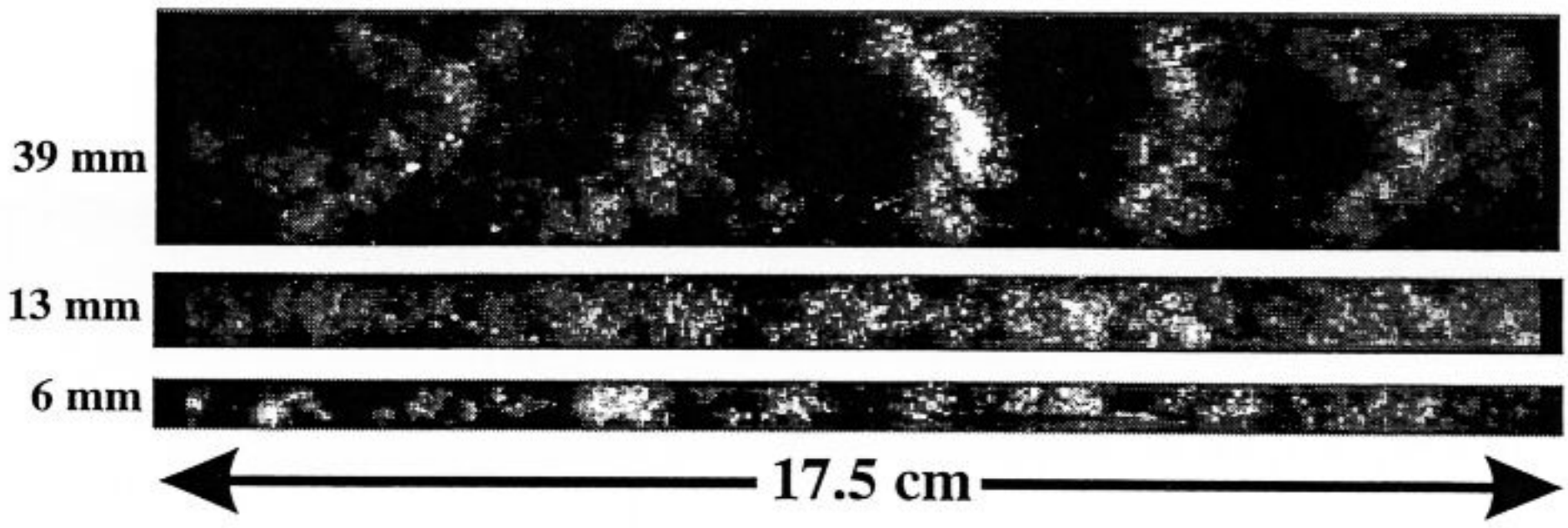


**Fig. 16.** Influence of the channel-width on the pattern. Driving amplitude: 1.8 cm, driving frequency: 3.3 Hz. Material: Monolayer of glass spheres, 0.6 mm diameter.

**Influence of the Roughness of the Channel.** The influence of the surface roughness was studied by preparing the bottom of the channels with glass spheres of different radii (Fig. 17). With rising roughness of the surface a pattern formation was prevented. If the ratio of the radius of the moving spheres to the radius of the ones glued on the bottom of the surface is around 10, pattern formation occurs. This indicates that the possibility for rolling or sliding motion of the spheres is a prerequisite for pattern formation. For great dumping heights only the upper layers of the granulate are fluidized. The lower layers act as a solid–like surface with the roughness of the granulate and thereby prevent a pattern formation. The influence of the roughness on the motion may be demonstrated by "cooling" a fluidized granulate by decreasing the driving frequency. Fig. 17 shows the patterns consisting of clusters of a real granulate (grains of seed) in three synchronously vibrated channels of different roughness after such a "cooling". A large roughness hinders the motion in the co–moving system, and decreases the distance of the clusters observed after the "cooling" process.

**Influence of the Driving Amplitude.** The influence of the driving amplitude on the pattern may be demonstrated by the "cooling" process and is shown in Fig. 18. The distance of the cluster after "solidification" increases with the driving amplitude, i.e. with the amplitude of the motion of grains in the co–moving system. The significant difference in the graphs of the seed grains and the glass spheres is not surprising because of the difference in all relevant properties of the two materials. Nevertheless, the behaviour of a real granulate is not totally different from the behaviour of the glass spheres in this experiment.

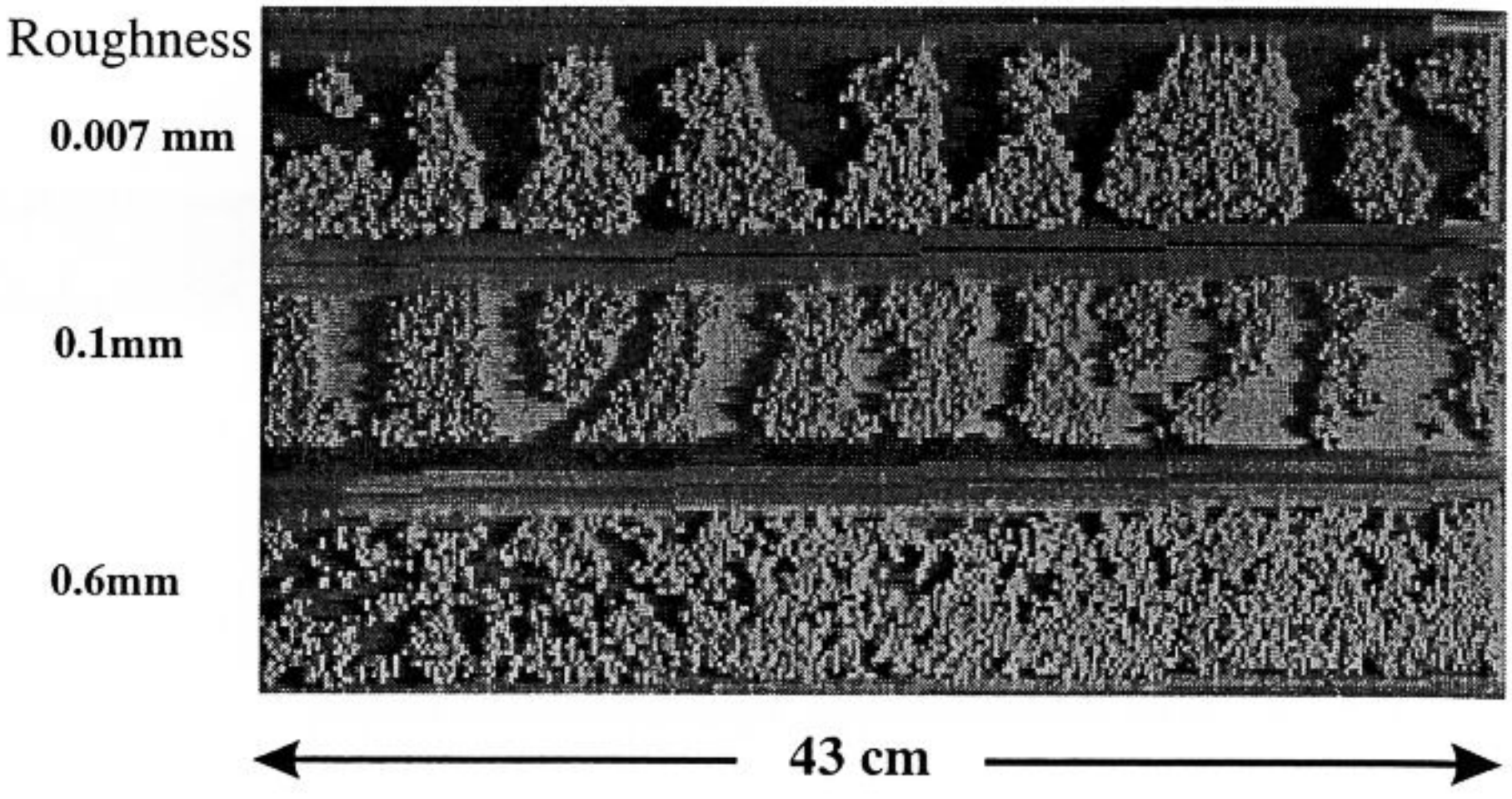


**Fig. 17.** Influence of the roughness of the channel on pattern. Material: Mustard seeds (1-2 mm diameter), driving amplitude: 2 cm, solid fraction: 0.44

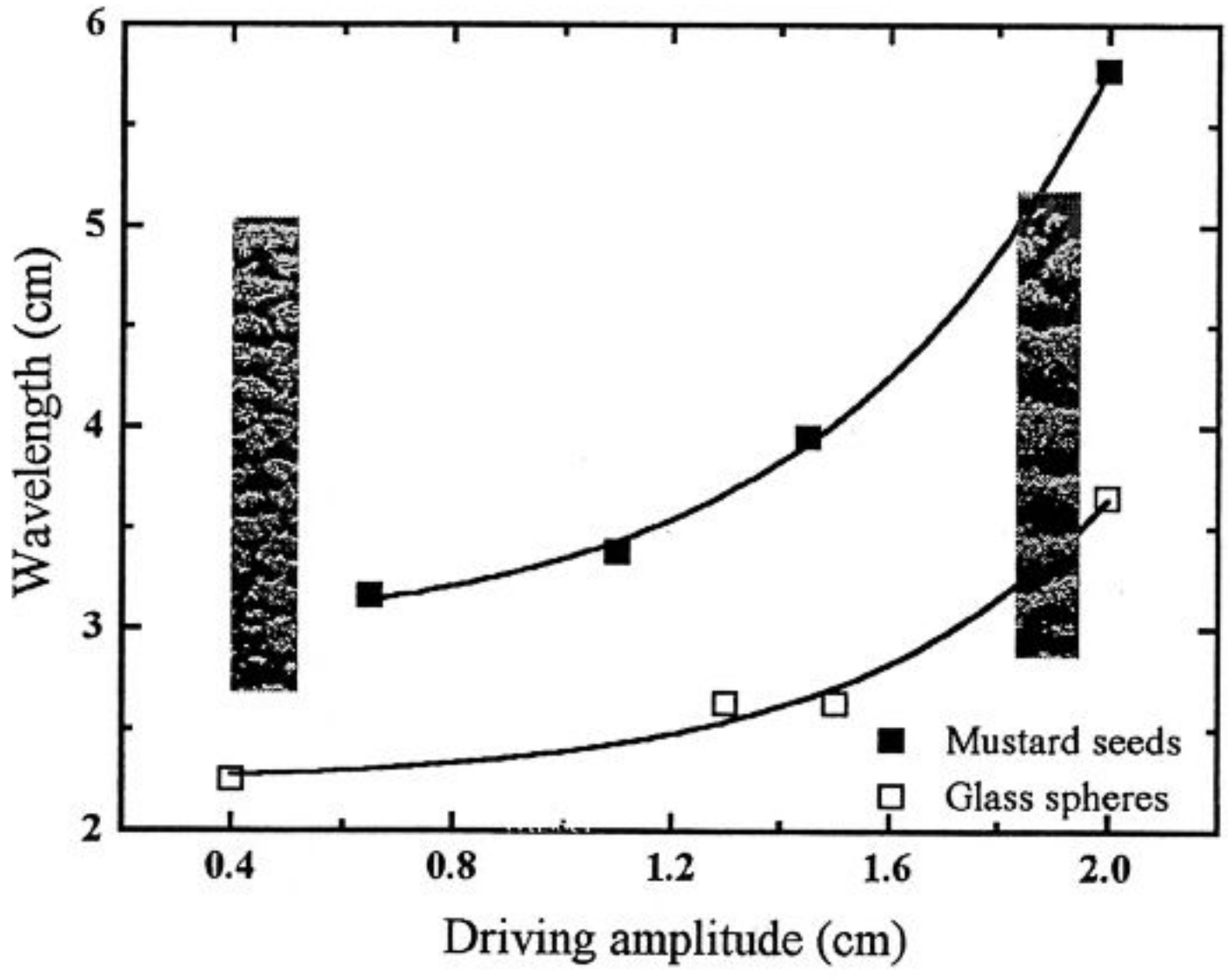


**Fig. 18.** Influence of the amplitude on clustering observed by "cooling". The images in the figure are taken from mustard seeds.

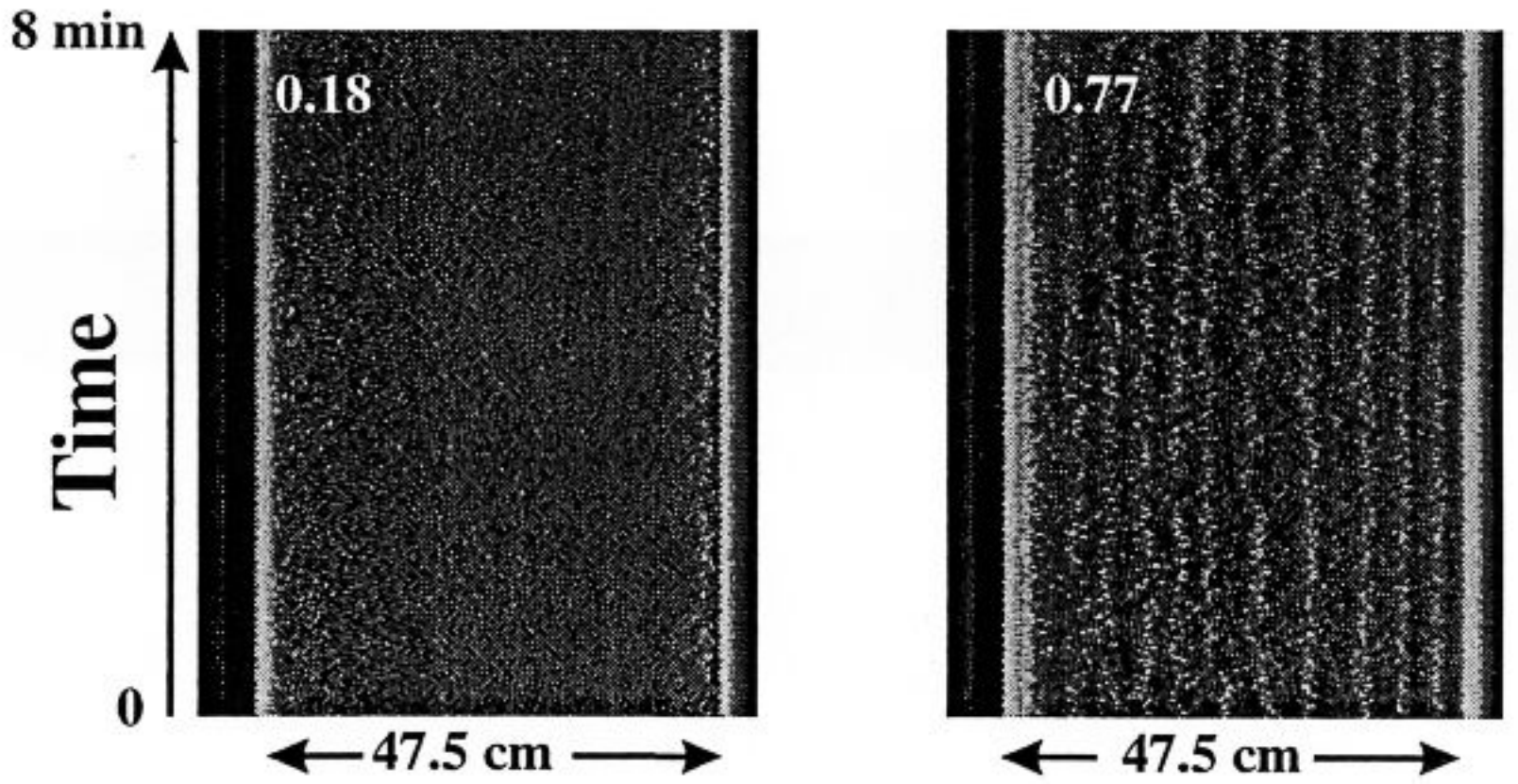


**Fig. 19.** Influence of the solid fraction on pattern formation. Material: Glass spheres of 1 mm diameter. Frequency: 4.5 Hz, amplitude: 1.2 cm.

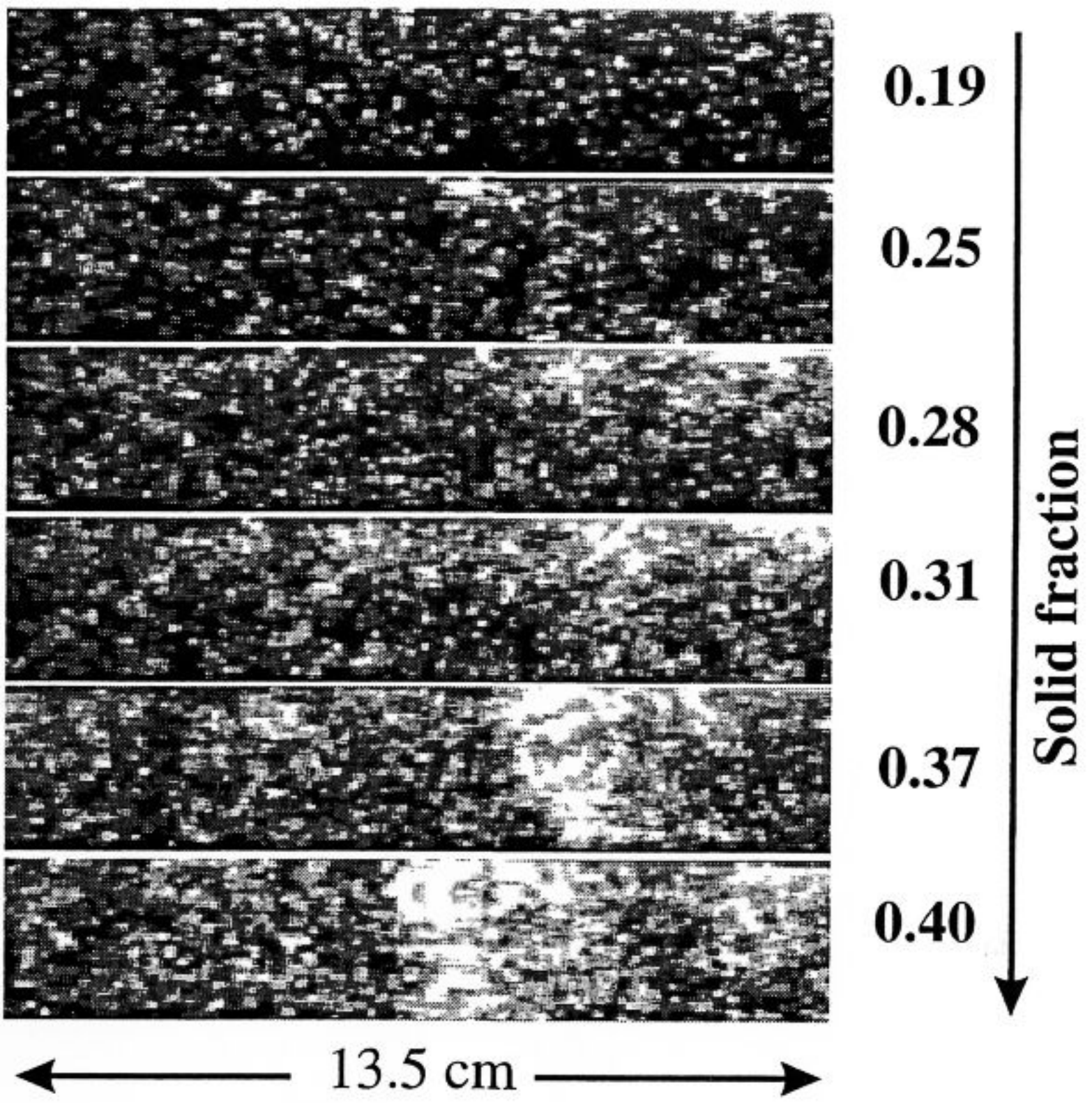


**Fig. 20.** High speed images below and above the transition point to clustering. Material: Glass spheres 1 mm diameter. Frequency: 3.5 Hz, amplitude: 1.2 cm.

**Mechanism of Pattern Formation.** In searching for a mechanism for the pattern formation we focus on a 2-dimensional system similar to those in Fig. 17 and Fig. 18. This means that we use a system with less than one monolayer. Depending on the solid fraction we have recorded space time diagrams from the intensity of one line from the images (Fig. 19). We used gracing incidence for the light. Above a critical value of the "solid fraction" we observe patterns, which are nearly stable in space and time.

By using an illumination similar to the one in Fig. 17 one can capture a representative number of single grains. We demonstrate, that the patterns are periodical changes in the granulate density (Fig. 20). By starting the vibration with grains distributed uniformly in the channel one can identify the clustering by comparing consecutive images. Pattern formation (clustering) starts above a critical value for the solid fraction. Near the critical value the interaction of clusters is observable. The exact determination of the transition point from a statistical independent motion to clustering will require the determination of the local position of the spheres by image processing.

## Pattern Formation under the Influence of Circular Vibration

In this section we now extend the above–mentioned linear horizontal vibration, where stripe–like patterns were found, to an orbital vibration. It is the typical motion which can be found in the late stages of never–ending boring dinner conversations. Under such circumstances people often start swirling their glasses in which some table water, wine, beer or even cognac might be left. In most cases the performed motion ends up to be an almost perfect orbital vibration which is horizontally aligned by the table. For a physicist this situation yields the advantage that he or she can focus on phenomena that arise in this kind of driven system. In a cognac glass i. g. gravity driven finger patterns appear in the region where the evaporated alcohol again condenses. In the context of this presentation we study a system which is unlikely to be present after dinner: a granular material. For a thin layer of sand it is found that it behaves like a solid at low rotation frequencies $f_d$. As $f_d$ exceeds a critical value the granular material fluidizes, which may lead to spiral patterns as shown in Fig. 21.

To uncover the underlying physics of this system we restrict our examinations to a monolayer of spheres and small numbers of particles $N$ with a rather large diameter $D$. Here, we review measurements that were performed in two different configurations: a circular dish and an annular channel. A transition where the sense of rotation of the cluster changes due to the number of particles is found in both: For small $N$ the particles follow the direction of the swirling motion (rotation) whereas the sense of rotation inverses (reptation) when $N$ exceeds a critical number. The experimental results are compared with a two–dimensional molecular dynamics simulation in the case of the circular container, and with a one–dimensional model for the annular channel.

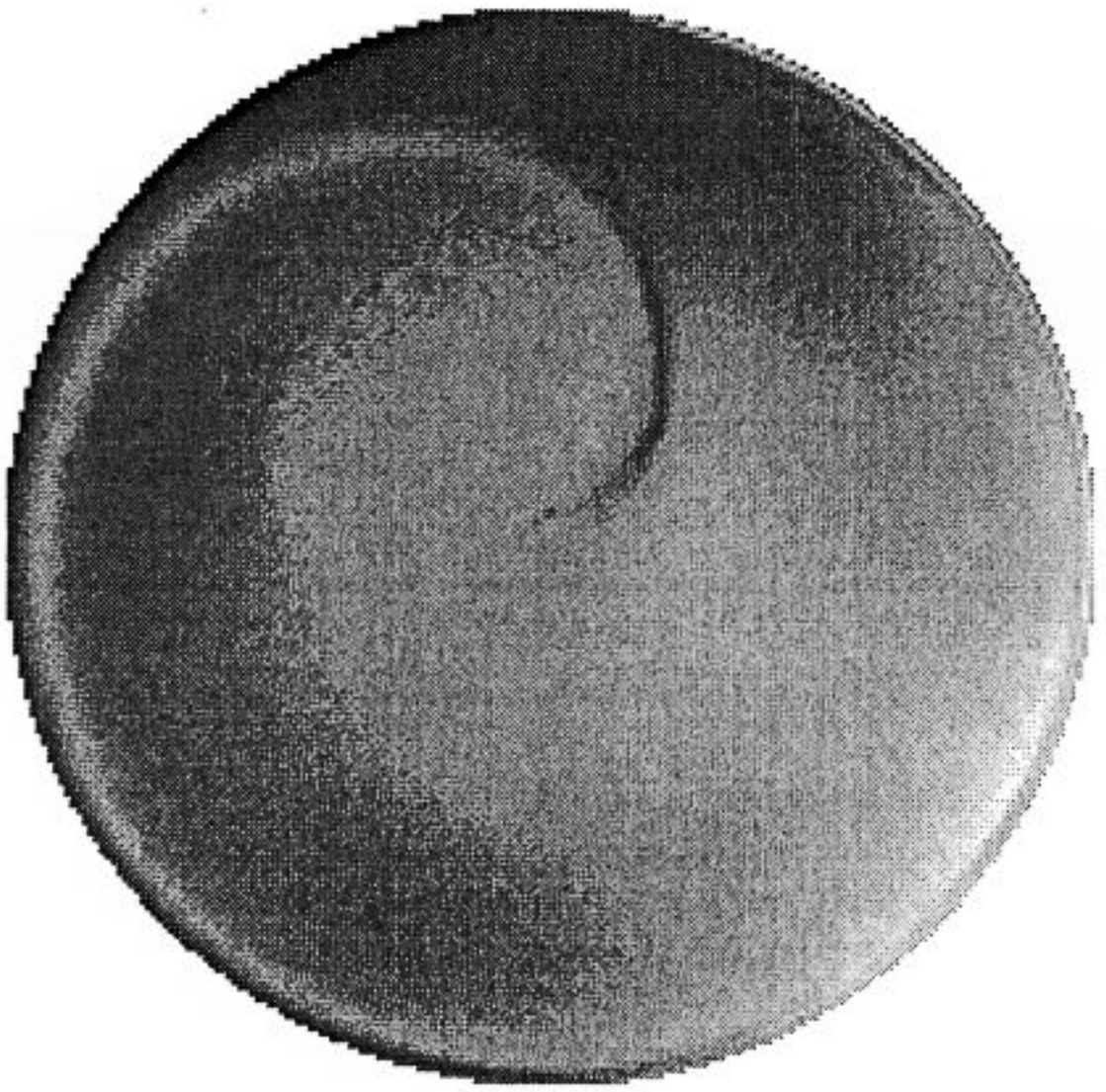

**Fig. 21.** Inverse image of a sand spiral obtained by swirling a thin layer of sand (size of circular container: 90 mm, frequency of driving: 3.63 Hz, amplitude of driving: 12.70 mm, diameter of sand beads: 50-150 $\mu$m, mass of sand: 13.2 g).

**Experimental Setup.** To investigate the behaviour of spheres under horizontal orbital vibration we used an adjustable reciprocating orbital shaker (Thermolyne AROS 160). In this apparatus every point $(x, y)$ on the swirling table moves counterclockwise on a circle in the laboratory frame:
$x = A_d \cos(2\pi f_d t)$ and $y = A_d \sin(2\pi f_d t)$, where $A_d$ is the driving amplitude of the shaker, $f_d$ the driving frequency and $t$ the time. In the following experiments $A_d$ is set to two different values: 9.53 mm and 12.70 mm. $f_d$ is in the range from 0 to 4.5 Hz. This kind of orbital vibration yields no center of rotation and every point feels the same centrifugal acceleration. As can be seen in Fig. 22, the setup is fixed on a heavy marble table to avoid internal vibrations. As containers we used a Petri dish and an annular channel. The Petri dish has an inner radius of 45 mm. The annular channel is milled out of Perspex. The outer radius of the channel is 50 mm and the width 10.5 mm, respectively. A CCD–camera (Sony XC–77RR–CE) on top of the setup allows visualization of the particle dynamics in the co–moving frame. A ring–shaped lamp (Schott KL 1500 electronic) and an annular neon light (Philips TLE Cool White) illuminates the scene. For the investigations in the circular container we use ceramic spheres of diameter $d = 12$ mm. The experiments in the annular channel are performed with precision spheres of different materials: bronze ($10.00 \pm 0.11$ mm), brass ($10.00 \pm 0.11$ mm), Polyurethane

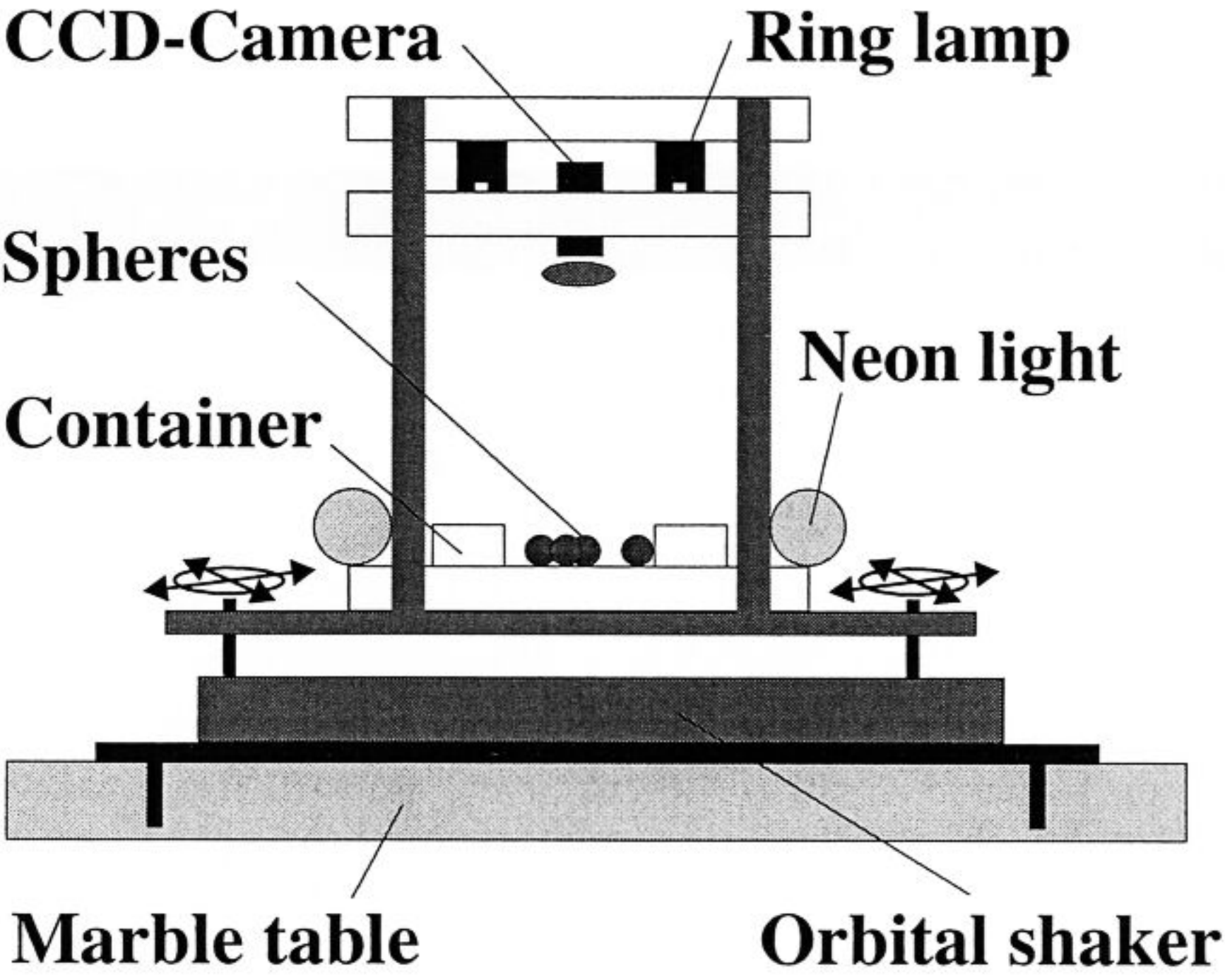


**Fig. 22.** Experimental setup for circular vibration.

(PUR, (9.85–10.10 mm)) and two types of Soda lime glass (glass): polished ($10.00 \pm 0.02$ mm) and deadened ($10.00 \pm 0.02$ mm).

**Experimental Results for the Circular Dish.** We now present results on the dynamics of the ceramic spheres in the circular dish. $A_d$ was set to 9.53 mm and $f_d$ to 2.5 Hz. Fig. 23(a) – Fig. 23(f) show the temporal evolution of 26 spheres in the co–moving frame. The momentary acceleration is indicated by the white arrow in each image. The arrow is obtained by drawing a line from a marker (small white cross) through the center of the Petri dish. The marker is fixed on a glass plate which is stationary in the laboratory frame and in between the dish and the camera. The position of the glass plate is adjusted in such a way that the marker circles around the center of the container when visualized in the co–moving frame. The snapshots were taken every 80 ms which corresponds to a time interval of $(5 f_d)^{-1}$. Thus, Fig. 23(a) and Fig. 23(f) belong to the same phase of the swirling cycle. By tracing the position of a single sphere in the cluster one finds that the sphere moves in the direction of the orbital shaking.

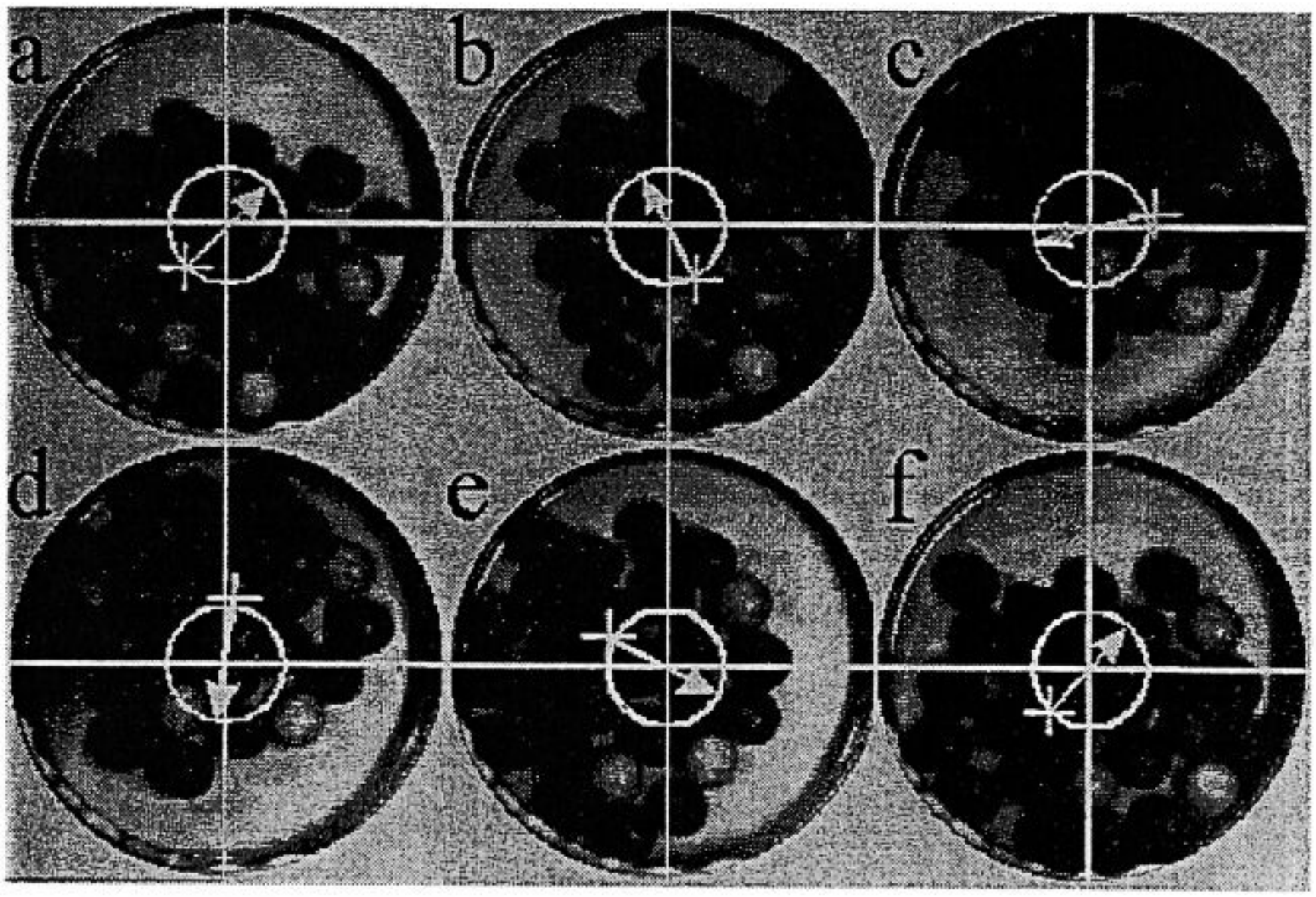


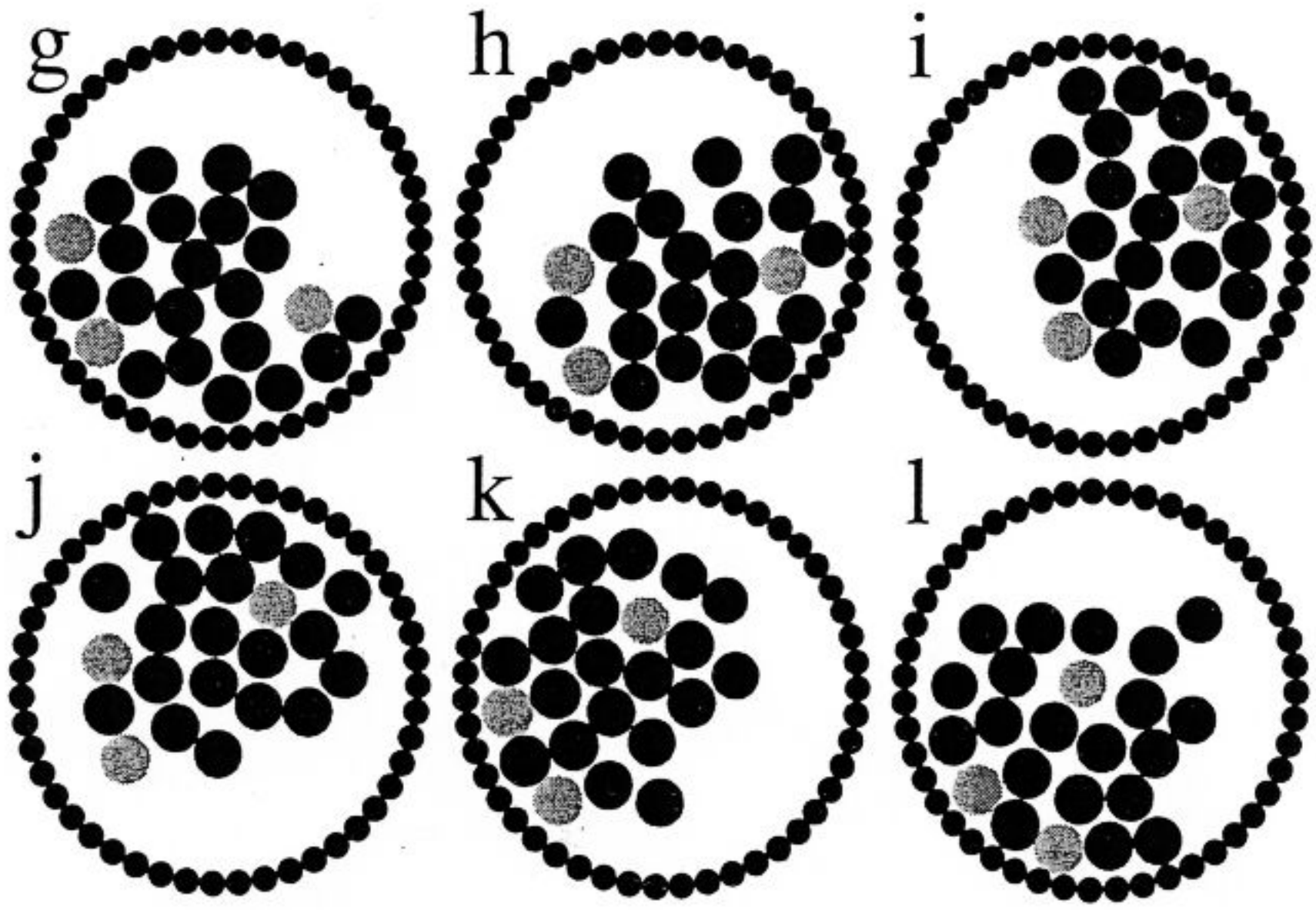


**Fig. 23.** Temporal behaviour of 26 spheres during one cycle of the orbital vibration (Scherer et al. 1996). The arrow indicates the direction of the momentary acceleration in the experimental snapshots ((a) – (f)). The lower six figures ((g) – (l)) correspond to the molecular dynamics simulation. Frequency of driving: 2.5 Hz, diameter of spheres: 12 mm.

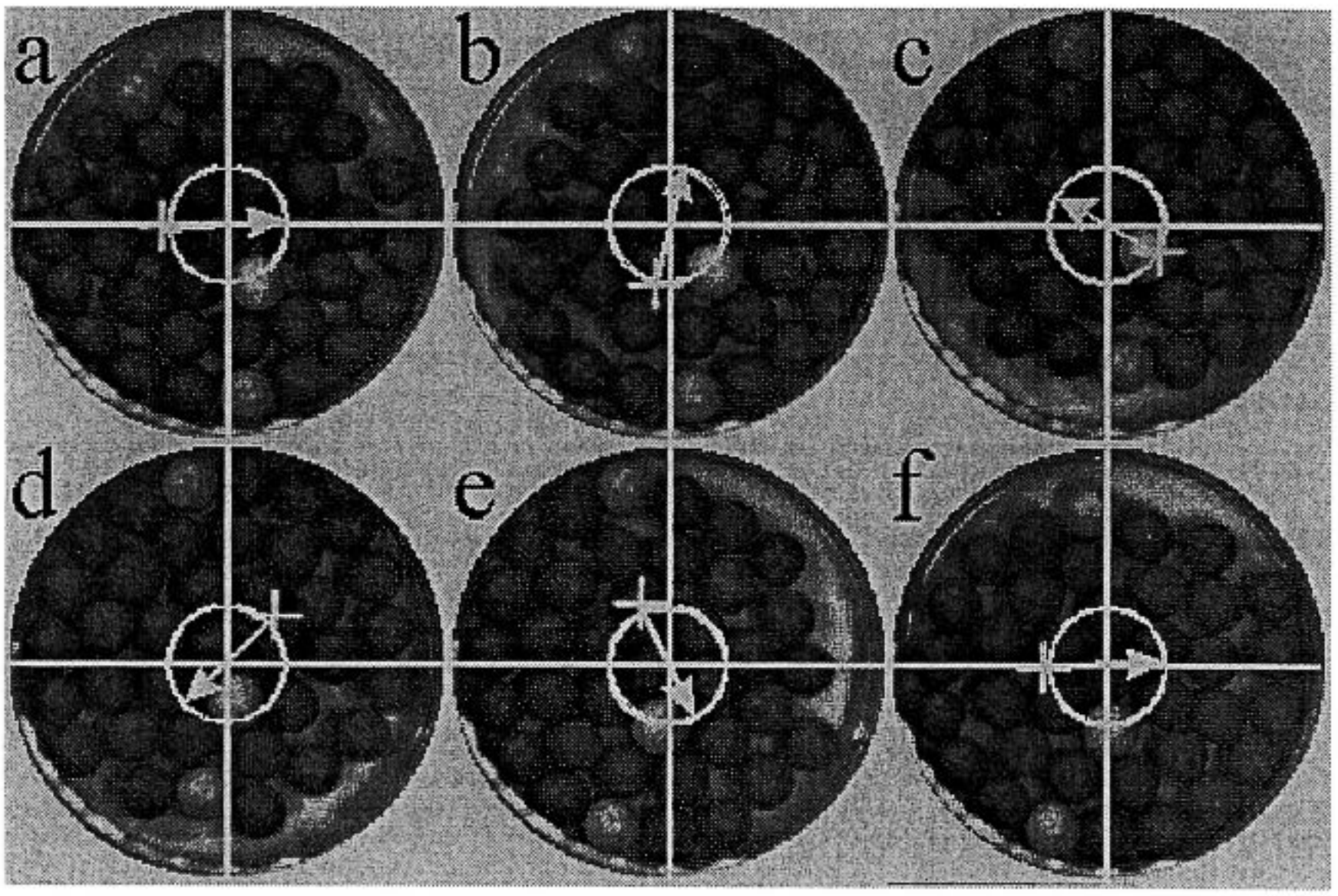


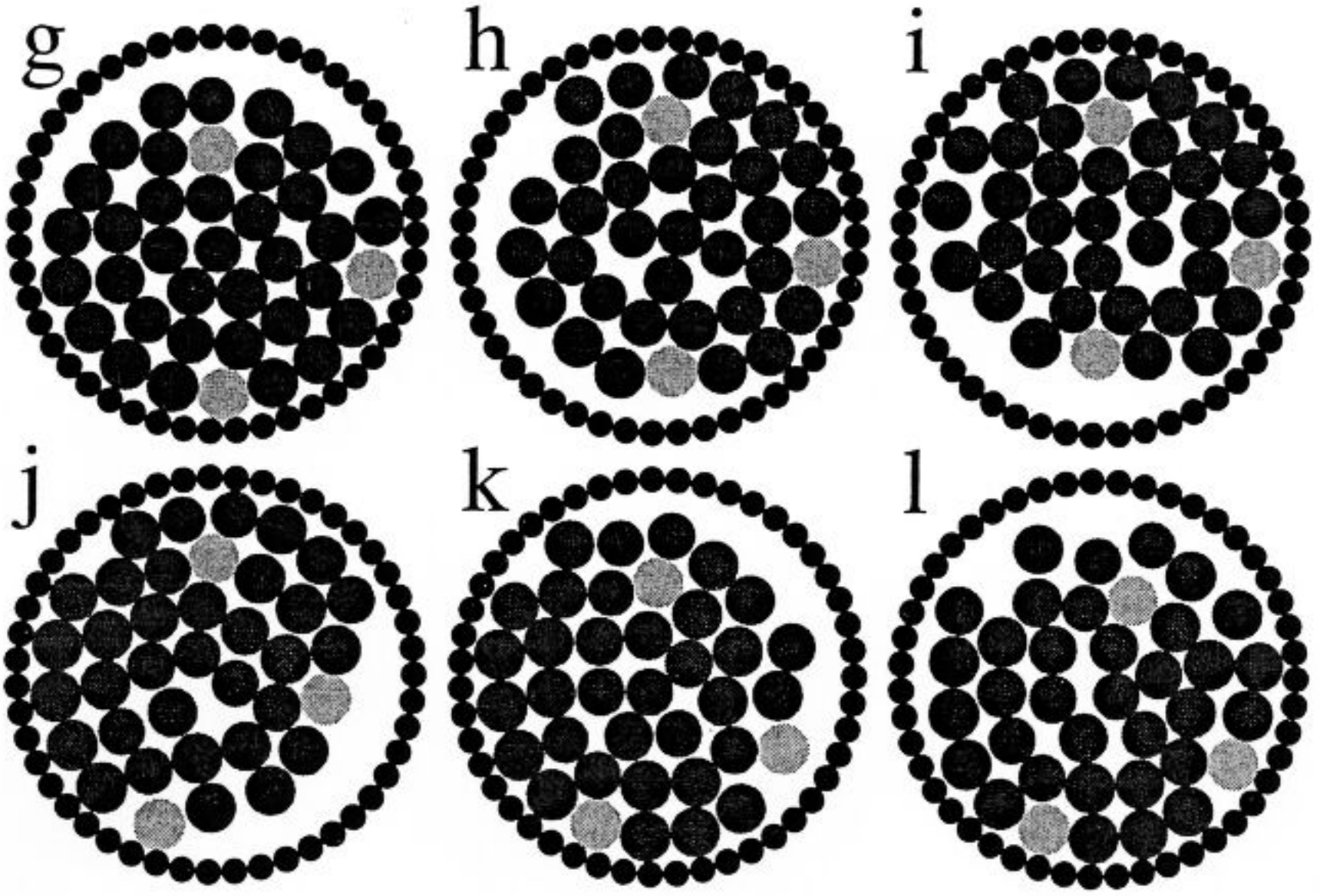


**Fig. 24.** Temporal behaviour of 37 spheres (Scherer et al. 1996). (a) – (f): experiment, (g) – (l): molecular dynamics simulation.

This behaviour is observed for all spheres and results in a global rotation of the cluster in the same sense as the external driving. This state we call rotation-mode. The experimental system has been compared to a two–dimensional molecular dynamics simulation. For details on the numerical procedure see the paper Scherer et al. (1996). Fig. 23(g)–Fig. 23(l) shows the same qualitative behaviour as the experiment.

For a higher number of spheres we observe a change in the dynamics of the cluster. Fig. 24(a)–Fig. 24(l) show the behaviour of 37 spheres for both the experiment and the numerical simulation. Here, the spheres move clockwise despite the counterclockwise motion of the shaking. We call this different state reptation-mode.

To quantify the dynamics of the cluster we measured the time needed by a single sphere close to the boundary of the Petri dish to circumnavigate the container. This gives a frequency of rotation $f_s$ as a function of the number of particles $N$. The open circles in Fig. 25 represent these measurements. It can be seen that when $N$ exceeds 24 $f_s$ decreases. At a critical particle number of 32 we observe a change in the sense of rotation of the cluster. Increasing the number of particles gives a higher frequency of rotation whereas the motion again slows down at very high particle numbers. We compare this findings with measurements obtained by the molecular dynamics simulation. Here, all positions and velocities of the spheres were taken into account and the frequency of rotation of all particles with respect to the center of mass of the cluster was calculated. The measurements are indicated by solid squares in Fig. 25. For sufficiently small $N$ it shows a good quantitative agreement with the experimental findings. For small particle numbers the experimental method for measuring the rotation frequency of the cluster breaks down because a single particle does not stay close to the boundary of the Petri dish. It has the tendency to migrate inwards.

**Experimental Results for the Annular Channel.** In a swirled annular channel it is found that there exists the same transition from rotation to reptation as seen in the circular dish (Scherer et al. 1997). Here we present measurements on the influence of the sphere material and the driving frequency for both modes, rotation and reptation. Figure 26 shows the response of the frequency of rotation on increasing the driving frequency for a particle number of 10. At this stage the one–dimensional array of particles is in the rotation mode. There is no significant influence of the material of the spheres: $f_s$ increases linearly as $f_d$ is set to higher values. In contrast, a cluster of 25 spheres shows a different behaviour (Fig. 27). The array is now in the reptation mode. While increasing the driving frequency the spheres revolve the channel with a higher frequency. This behaviour does not seem to depend on the material at low frequencies. But it breaks down when $f_d$ exceeds a critical value of 2.5 Hz. At this stage deadened glass slows down while the frequency of rotation of PUR still increases.

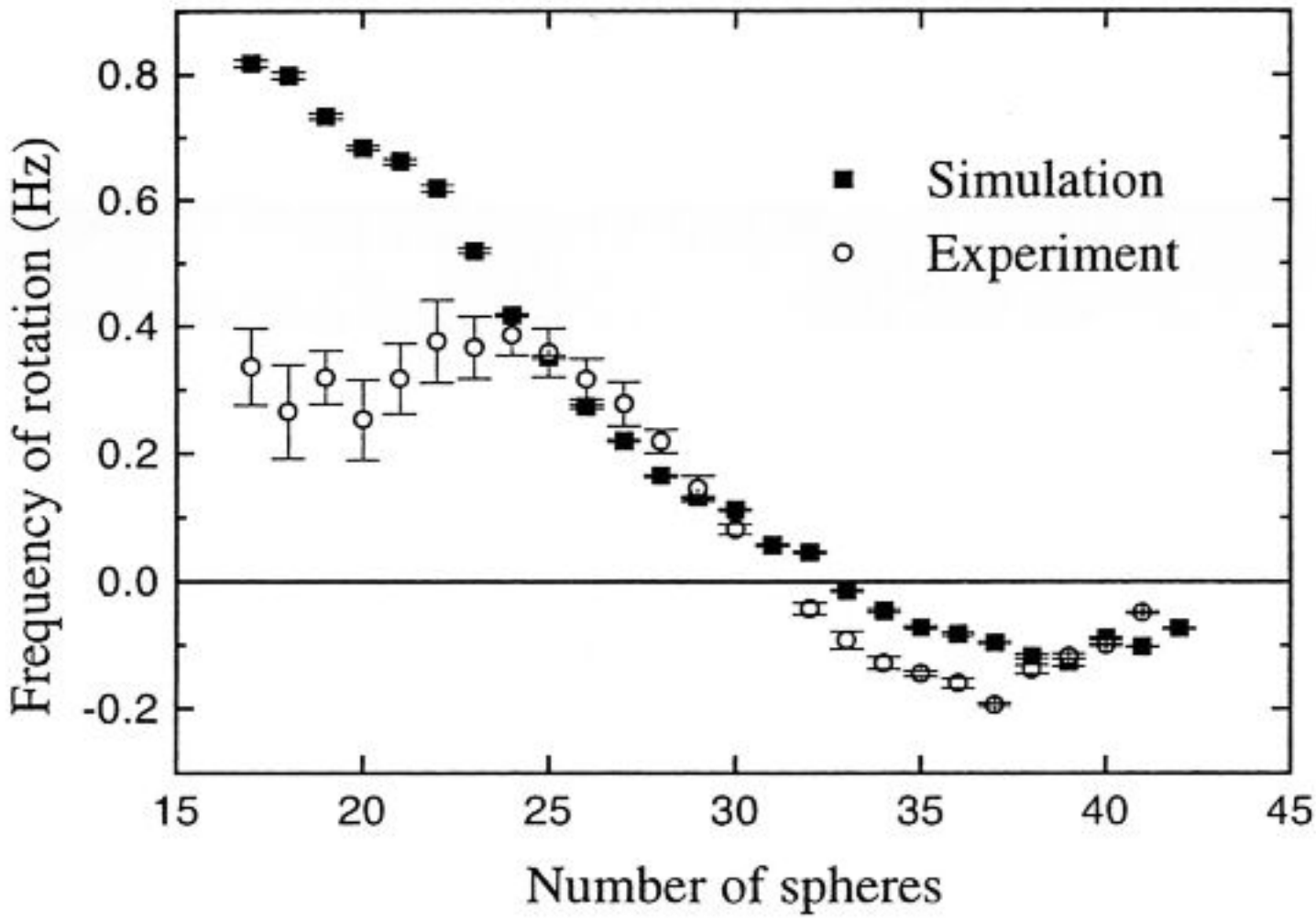


**Fig. 25.** Frequency of rotation of the cluster (Scherer et. al 1996). The solid squares show the results of the molecular dynamics simulation, while the open circles represent the experimental measurements. For a critical number of 32 spheres there is a reversal in the sense of rotation of the cluster.

To get a closer picture of the dynamics of the spheres we visualize the trace of the center of each sphere. Fig. 28 shows space–time evolutions for four different particle numbers. As particles bronze spheres were used. The amplitude of driving is set to 9.53 mm; the frequency of driving is 2.5 Hz. The horizontal axes of each image belongs to the space coordinate and the vertical axes represent time, respectively. Time evolves from bottom to top. The centers of mass of the spheres appear black. At low particle numbers ($N = 10$) we notice that there are almost no collisions. Each particle has a slow translatory motion which is superimposed by a fast back and forth motion of the sphere. Near the critical point where the transition from rotation to reptation ($N = 25$) occurs we observe strong fluctuations in the motion of the spheres. At higher solid fractions the spatial–temporal behavior becomes more ordered. Fig. 28 gives an example for $N = 24$. The highest possible number of particles in this experimental case is $N = 28$. Here, the frequency of rotation is very slow; for a limited part of the period of the external driving the particles even move backwards. The dynamics of a single sphere can be

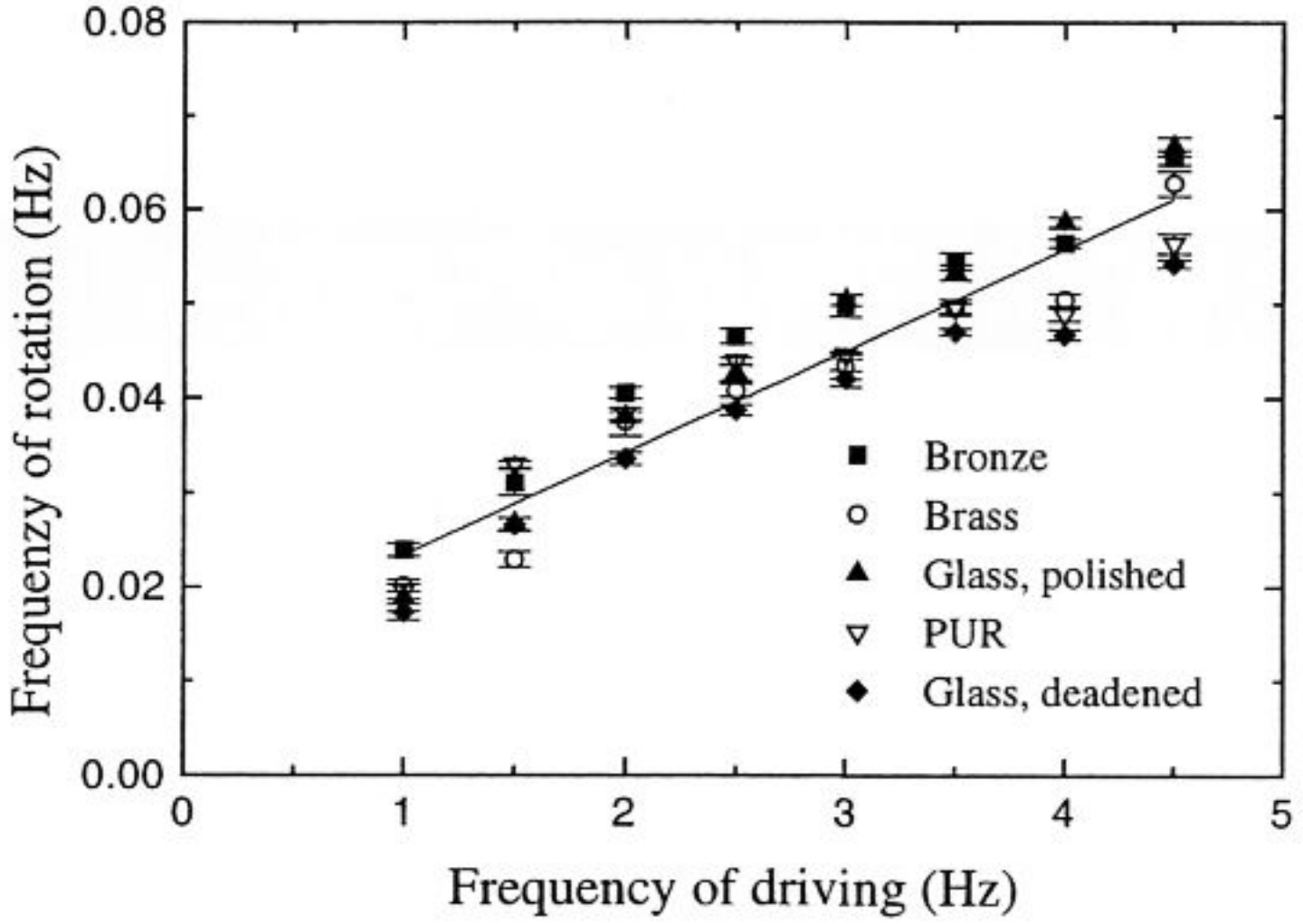


**Fig. 26.** Dependence of the frequency of rotation of the spheres on the driving frequency for different materials (Scherer et al. 1997). The number of spheres in the annular channel is 10. The line serves as a guide to the eye.

described by a one dimensional model,

$$\ddot{\phi} + \eta\dot{\phi} + \epsilon \sin(\phi - t) = 0, \tag{2}$$

where $\phi$ is the position of the sphere in the channel, $\eta$ an idealized viscous friction, and $\epsilon$ the ratio between the driving amplitude and the distance from the center to the middle of the annular channel. The time t has been made dimensionless by multiplication with the angular frequency of the driving.

It can be shown (Scherer et al. 1997, Scherer 1998) that for $\eta/\epsilon < 1$, which is the regime of the experimental setup, there exists a solution where the sphere has a slow drift superimposed by a fast oscillatory part,

$$\phi(t) = \frac{\epsilon^2}{2(1+\eta^2)}t + \frac{\epsilon}{\sqrt{\eta^2+1}} \sin(\phi - t + \arctan\eta). \tag{3}$$

This is in good agreement with the experimental findings. Measuring the drift velocity of the slow translatory motion and the amplitude of the fast oscillation give two independent methods to determine the coefficient of viscous friction $\eta$. For bronze spheres, which are swirled with a driving amplitude of 9.53 mm and a driving frequency of 2.5 Hz (see Fig. 28), we have obtained $\eta = 0.7$ for both cases.

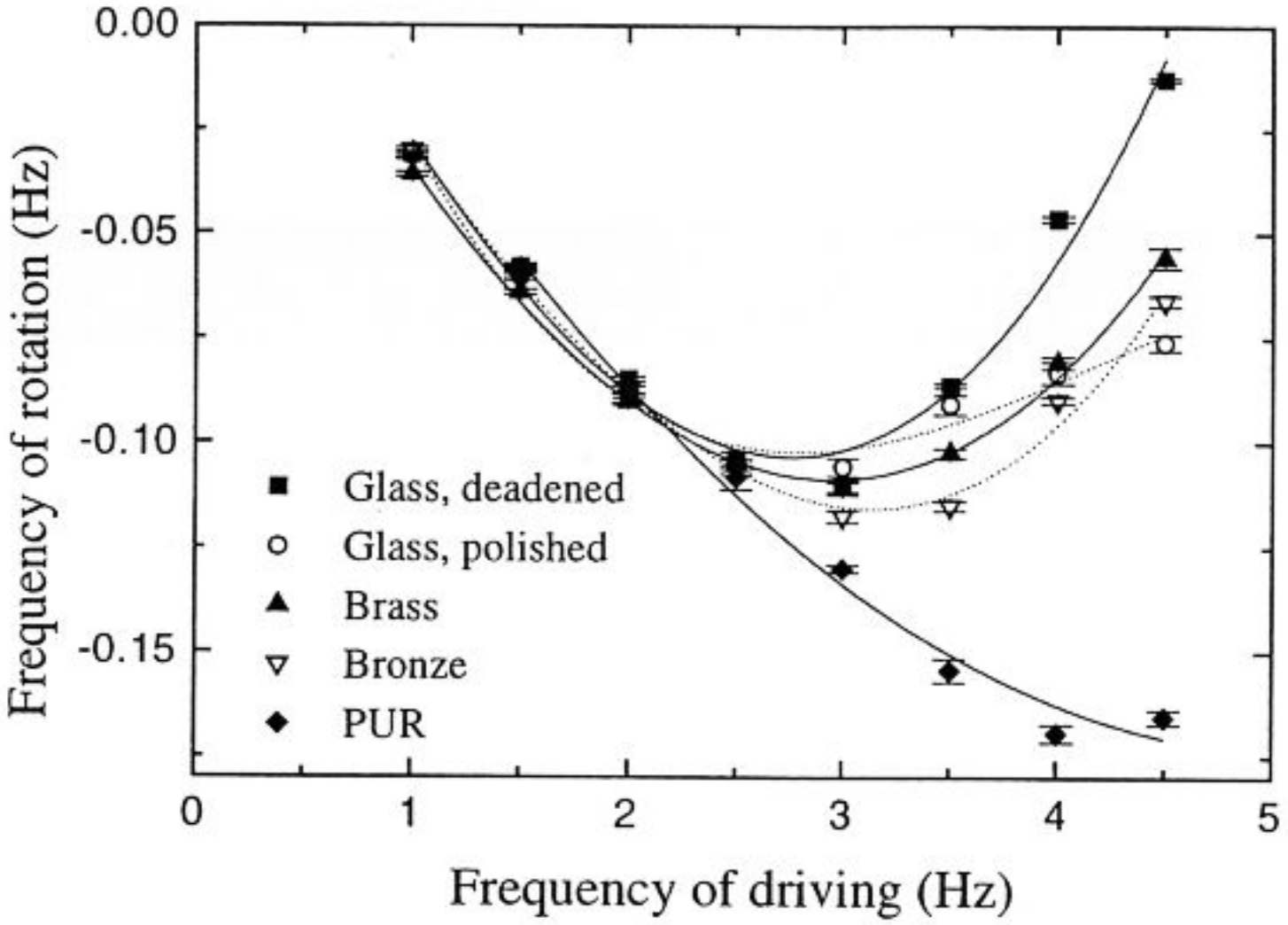


**Fig. 27.** Dependence of the frequency of rotation on the driving frequency for 25 spheres (Scherer et al. 1997). All curves have parabolic shape except for polished glass where a cubic fit is more reasonable.

We use Eq. (2) with $\epsilon = 0.21$ and $\eta = 0.7$ to simulate the behaviour of many particles[1] (Scherer et al. 1997). When there is a collision between two neighbouring particles 1 and 2, we calculate their new velocities $v_1'$ and $v_2'$ from

$$\begin{pmatrix} v_1' \\ v_2' \end{pmatrix} = \begin{pmatrix} 0 & \nu \\ \nu & 0 \end{pmatrix} \begin{pmatrix} v_1 \\ v_2 \end{pmatrix}, \tag{4}$$

where $v_1$ and $v_2$ are the velocities of both particles before the collision, and $\nu$ is the coefficient of restitution. Fig. 29 shows $f_s$ normalized by $f_d$ as a function of the number of spheres. The solid squares are the experimental values obtained for bronze spheres. The simulation starts with elastic collisions, which means $\nu = 1$ (solid circles). In disagreement with the experimental values, the frequency of rotation does not decrease when approaching the critical point where we observe experimentally a transition from rotation to reptation. Only for $N = 28$ we find a reversal in the sense of rotation. This behaviour changes dramatically when we set the coefficient of restitution to

[1] An interactive Java simulation of the numerical system can be found at URL http://comserv.urz.uni-magdeburg.de/~anp/safe/swirlsim/swirlsim.html. Various parameters like the coefficient of restitution or the number of spheres can be varied.

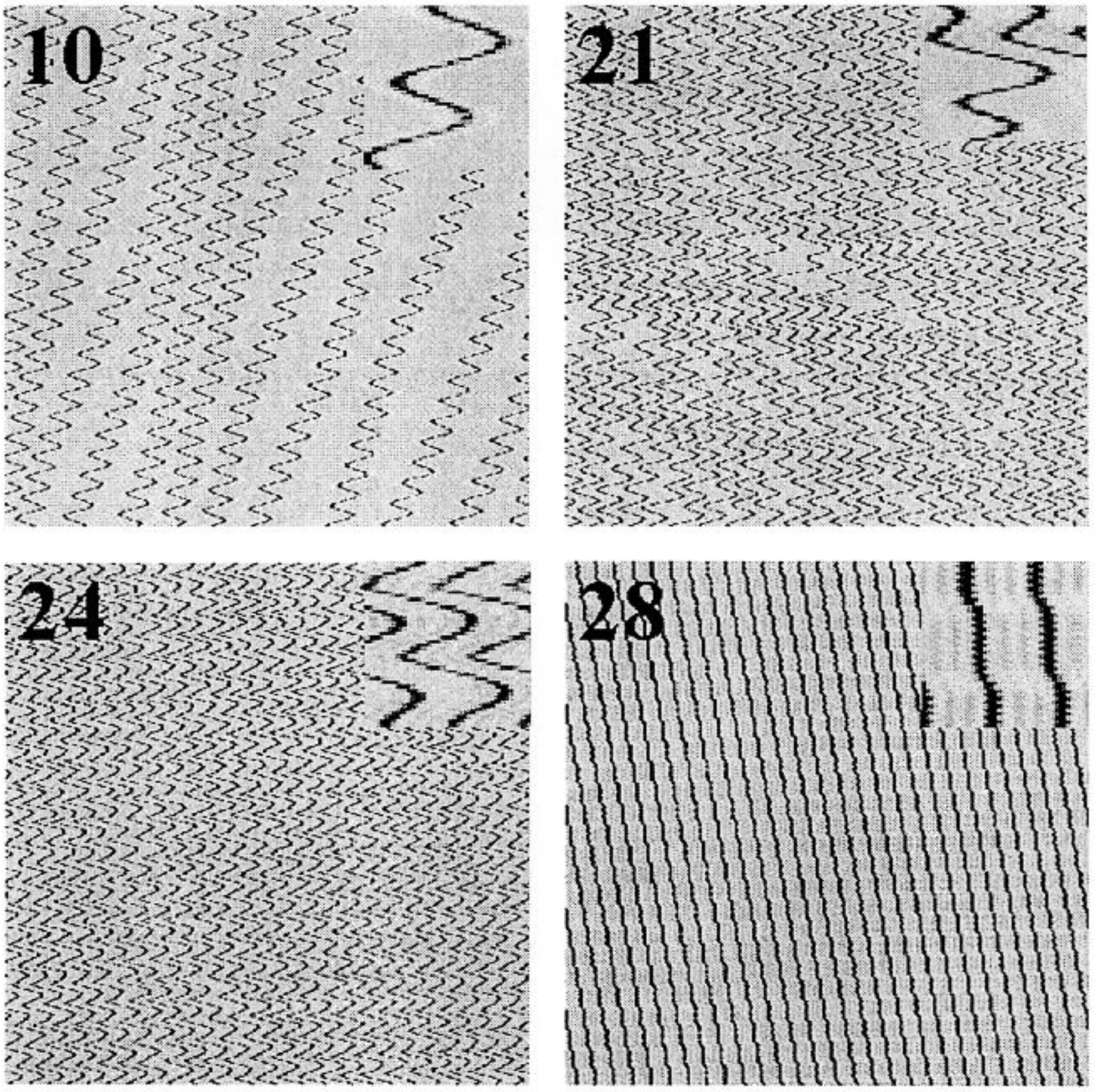


**Fig. 28.** Spatial–temporal evolution of the centers of the spheres (Scherer et al. 1997). The horizontal axes in each image is the space coordinate (0 to $2\pi$) while the vertical axes shows the time (0 to 10.24 s). The number in the upper left corner denotes the number of spheres in the annular channel. In the upper right corner a magnified section is given. Material of the spheres: bronze, driving amplitude: 9.53 mm and driving frequency: 2.5 Hz.

0.99 (open triangles). Here, we already get the correct qualitative behaviour. Varying $\nu$ we find that there is a good agreement for 0.7 (open circles).

We have tested a collision model where energy dissipation is introduced by reducing the relative velocity of both particles and an additional conservation of momentum (Scherer et al. 1997). Even in the case of completely inelastic collisions we were not able to reproduce the experimental results. This is due to the fact that not only normal collisions are important for this process. The

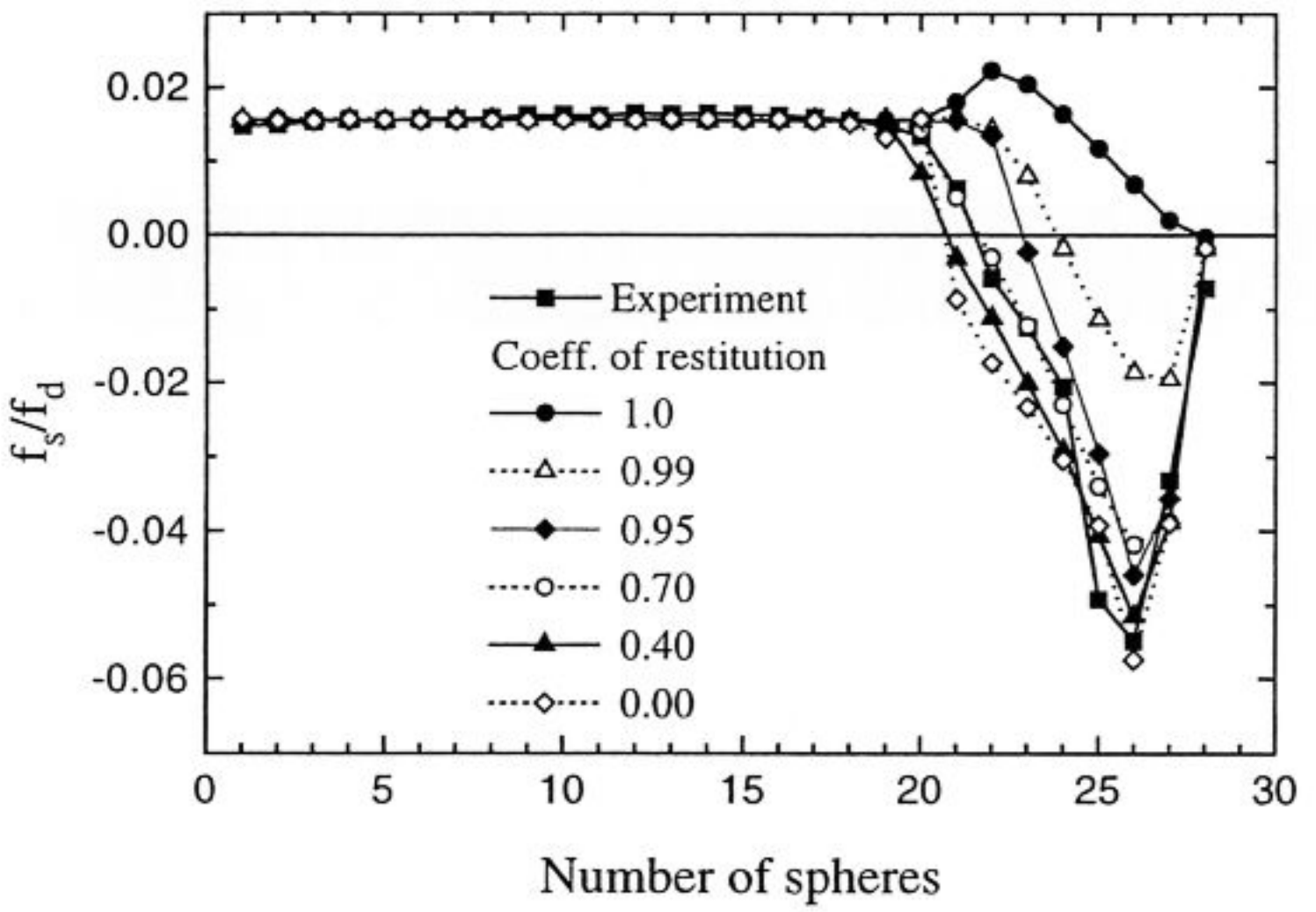


**Fig. 29.** Comparison of experimental results with numerical simulations of many particles in dependence of the coefficient of restitution (Scherer et al. 1997). The experimental conditions are the following: As sphere material we use bronze, $A_d = 9.53$ mm, and $f_d = 2.5$ Hz.

tangential shear at the contact points of the colliding spheres has to be taken into account as well. Thus, the dissipation of energy also depends on the spin of the particles and the collision process is governed by the absolute velocity of the spheres as modeled by Eq. (4).

In summary, we have presented measurements on the transition from rotation to reptation in granular material under horizontal orbital shaking. The experimental findings in the case of the circular dish are in good agreement with a two dimensional molecular dynamics simulation. This is of importance for processes in vibrational mills where the same effects occur (Yokoyama et al. 1996). To understand the underlying physics of this phenomena we have reduced our system to an annular channel. It was shown that material properties do not influence the dynamics in the rotation mode. In contrast we see a strong dependence on the sphere material in the reptation mode. This suggests that the granular dynamics is governed by binary collisions. We have confirmed this idea numerically. We first studied the dynamics of a single sphere. The results found by analysing a one–dimensional model were in good agreement with the experiment. A single sphere shows a slow translatory motion on which a fast back and forth motion of small amplitude is

superimposed. We have used these results to simulate a many–particle situation. It was found that elastic collisions do not give a transition from rotation to reptation whereas inelastic collisions confirm the experimental values accurately. The degree of accuracy depends on the coefficient of restitution.

We plan to study pattern forming processes like the spiral seen in Fig. 21. The experimental results should give a hint on how to model the basic dynamics of granular materials.

## Pattern Formation at the Interface of a Sedimenting Suspension

In many cases the air between granular particles can be neglected, and the granulate behaves in the same manner as it would under vacuum conditions. For reasons of convenience, most experiments are not performed in vacuum, however, and it is well known that the air might give rise to forces between the particles. These forces are much stronger if the air is replaced by water. If the resulting suspension is a dilute one, the characteristics of the granulate might become totally unimportant. The suspension behaves like a Newtonian fluid with a slightly increased viscosity, namely the viscosity coefficient increases by a fraction which equals 2.5 times the volume fraction $\Phi$ of the suspended spheres (Einstein 1906, Einstein 1911).

This is no longer true for more concentrated suspensions. Expanding the viscosity $\eta$ in terms of $\Phi$ one finds the coefficient of $\Phi^2$ to be dependent on the geometry of the flow (Batchelor and Green 1972, Batchelor 1977). This fact also explains why the result of viscosity measurements depend on the geometry of the apparatus (Pätzold 1980). If the volume fraction exceeds a certain threshold there occurs shear thickening i.e. the apparent viscosity increases with the shear rate. In this region, which was first described by Bagnold (1954), the suspension is clearly non–Newtonian. All these complications should be born in mind when interpreting the experimental results described below, namely the formation of patterns in a sedimenting suspension.

**Measurements.** The main problem for an experimental setup is how to prepare the initial situation with the denser material on top of the lighter one, and with a sufficiently flat interface between both phases. In our experiment we try to reach this situation by turning a closed Hele–Shaw–like cell around a horizontal axis (see Fig. 30).

The cell, a CCD–camera and a neon tube are fixed to a frame whose bottom bar is the rotation axis. This allows image analysis in the co–moving frame and ensures a homogeneous illumination at every stage of the pattern forming process. The length of the cell is 160 mm, the height 80 mm and the width 4 mm, respectively. The cell is filled with 2 g sand (which is a layer of about 2.5 mm height) and distilled water. As sand we used sieved spherical glass particles (Würth Ballotini MGL) with a diameter range of 71–80 $\mu$m. Its material density is given by 2.45 g/cm$^3$. The cell was rotated by

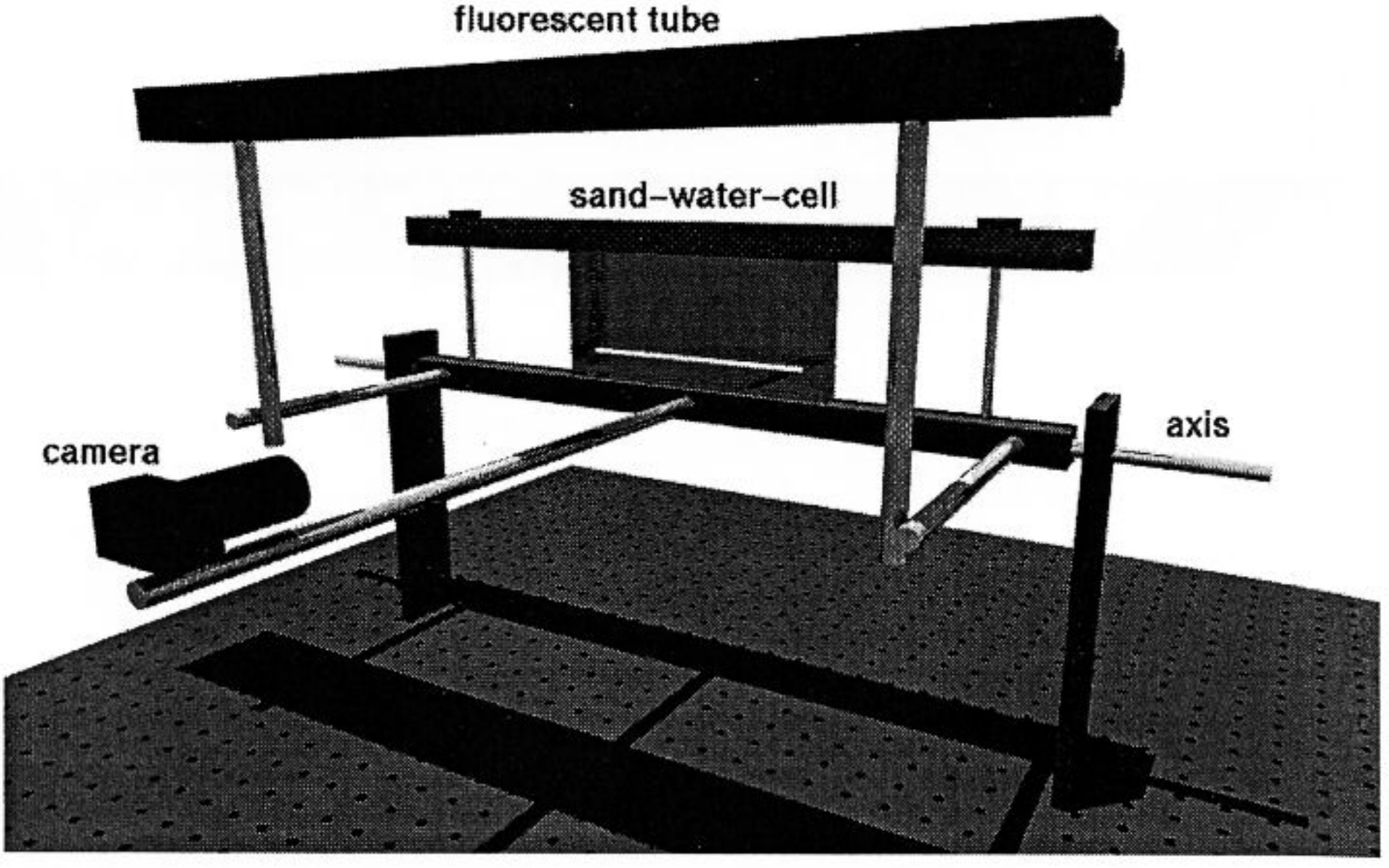


**Fig. 30.** Experimental setup for measuring sedimentation.

hand. To obtain reproducible results the vertical and horizontal acceleration is measured by acceleration sensors (ADXL05). When the cell passes a rotation angle of 170 degree, a light-gate triggers a number of snapshots. This moment defines the starting time for taking images every 20 ms for later analysis. The images have a dimension of 256 x 300 pixel. To achieve a reasonable resolution we focus only on a horizontal length of 61 mm at the middle of the cell. This gives a resolution of 4.9 pixel/mm. Fig. 31 shows five images of the sand-water cell sampled in time intervals of 60 ms. The first snapshot shows that the initial flat sand layer is modulated at small scales (Fig. 31(a)). These disturbances are enhanced and give rise to sand fingers as seen in Fig. 31(c). At later stages the fingers evolve to a mushroom-like pattern (Fig. 31(d) and Fig. 31(e)).

We have applied a threshold algorithm to obtain the water–sand interface. Starting at the bottom (water) and continuing to the top (sand) we look at every column of our digitized image to determine the point where the grey level exceeds a certain value. In this way we track down the interface of the pattern.

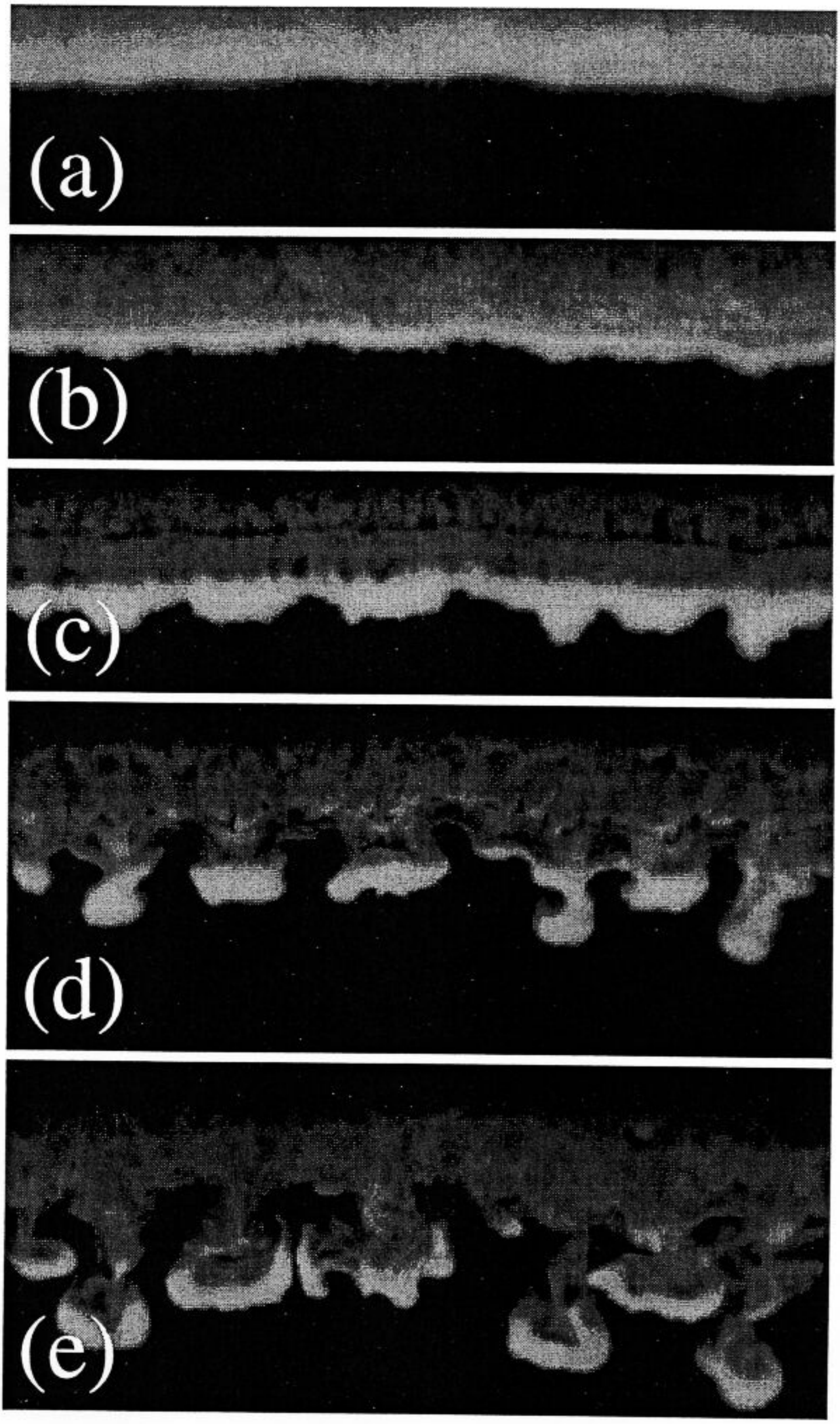


**Fig. 31.** Sand–water interfaces at a) 20 ms, b) 80 ms, c) 140 ms, d) 200 ms, and e) 260 ms after start of the experiment. The diameter range of the sand particles was 71-80 $\mu$m, and the total sand mass in the cell is 2 g. The frames show the middle part of the cell with a horizontal extension of 68 mm.

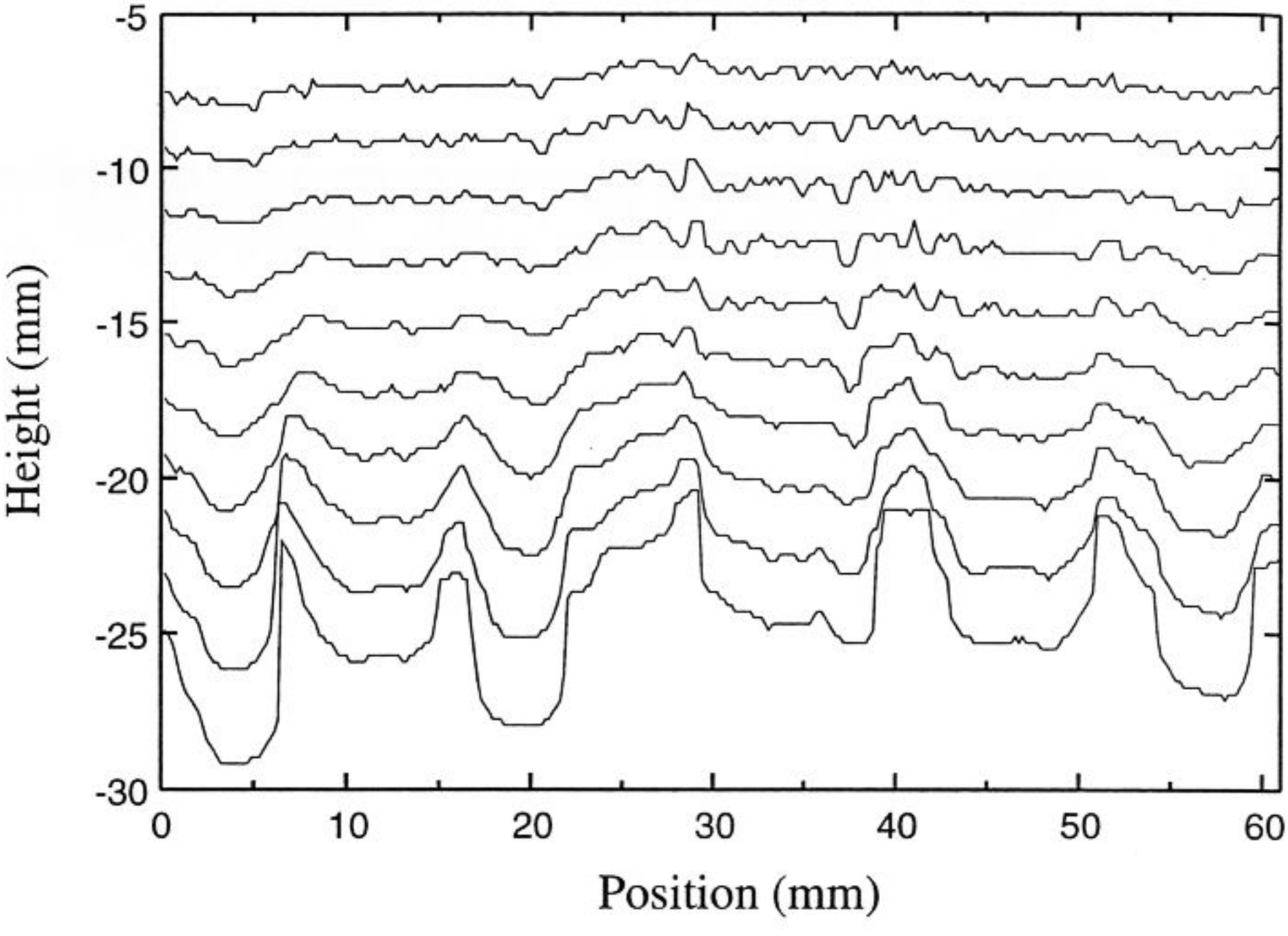


**Fig. 32.** Temporal evolution of the water–sand interfaces. The patterns are detected every 20 ms and plotted with a constant vertical offset of 1 mm. The experimental conditions are the same as in Fig. 31

Fig. 32 shows the temporal evolution of the front for the experiment in Fig. 31. Here the interfaces of all patterns are shown. While our detection method works well for the patterns during the first stages, namely small scale modulations and sand fingers, it gives erroneous results for the mushroom–like patterns. However, this is not crucial because those patterns are beyond the scope of the analysis that we want to perform here. A discrete Fourier transformation (DFT) gives the power spectrum of each interface. Fig. 33 shows the temporal evolution of the amplitude $A$ of a typical mode. It is seen that $A$ grows exponentially from the first image to $t = 200$ ms. By an exponential fit

$$A(k) = A_i(k) \exp(n(k)t) \tag{5}$$

we obtain the growth rate $n$ for every wave number $k$ in our spectra, where $A_i$ is the initial amplitude.

In order to test the reliability of our experimental setup we have performed 100 independent runs. We only analysed image series for which the time for rotating the apparatus 180 degrees was smaller than 450 ms. These 42 measurements (average rotation time: 404 ms $\pm$ 31 ms) were analysed to obtain a mean growth rate for each wave number.

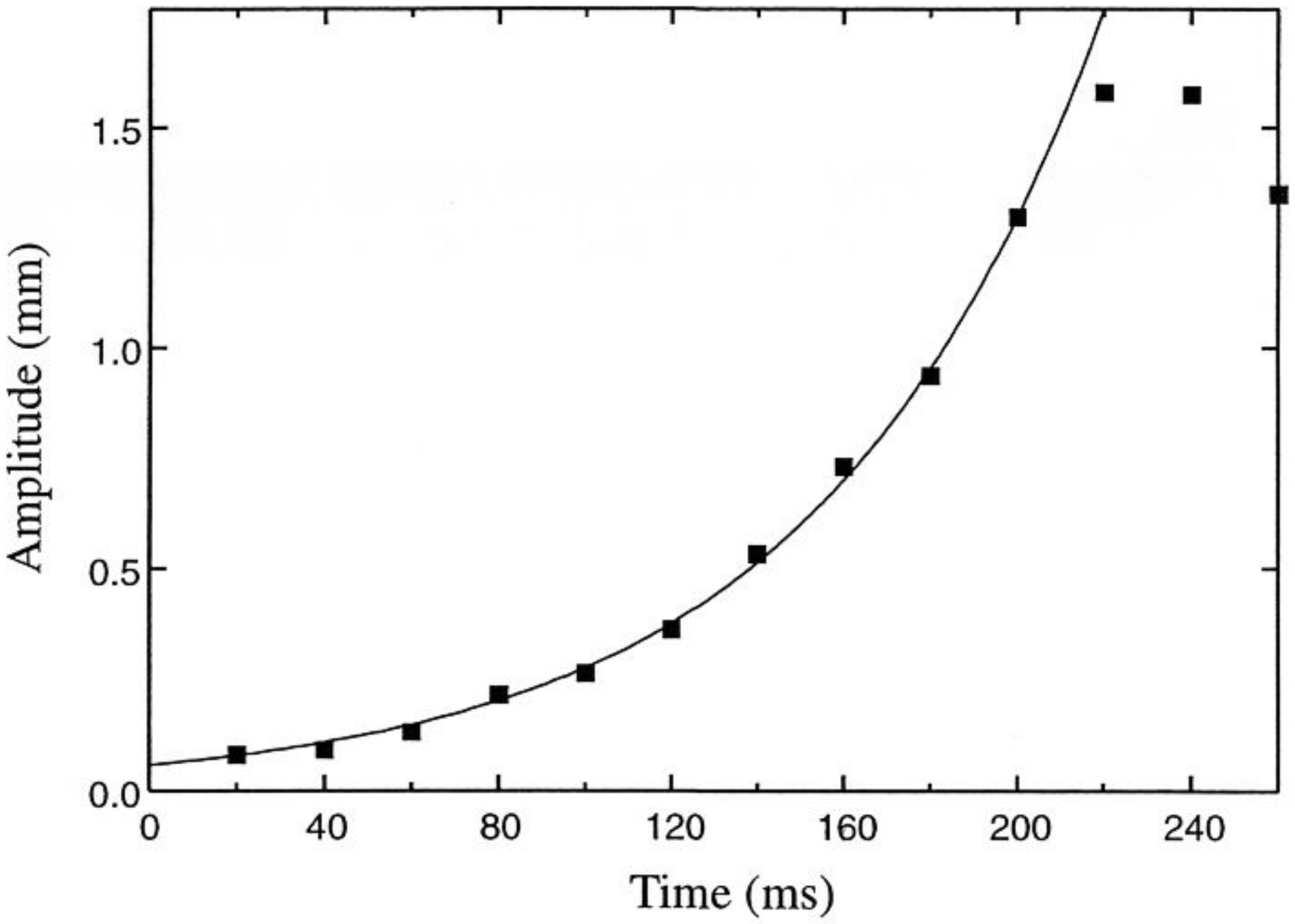


**Fig. 33.** Amplitude $A$ obtained from a DFT–analysis for a typical wave number (here $k = 7$ cm$^{-1}$) in dependence on time $t$. The solid line is yielded by a fit according to Eq. (5). The data correspond to Fig. 32.

**Results.** The square dots in Fig. 34 show the measured dispersion relation. It is seen that the growth rates increase with increasing wave number until they saturate at larger $k$. In the case of large wave numbers we did not obtain exponential fits for all experimental runs. This is due to the fact that the amplitude is very small and that we approach the limit of the resolution of our image processing.

An obvious question concerning the underlying mechanism of the pattern formation in our system is: How do different material parameters affect the dispersion relation? We have carried out experiments with different values for the total mass and different size distributions. Using 2 g, 4 g, and 8 g of sand we observe a small shift of all growth rates towards larger values with increasing mass of sand. This effect is independent of the wave number. Using three different size distributions 56-63$\mu$m, 71-80$\mu$m and 90-100$\mu$m we found that the mean particle diameter does not have any significant influence on $n(k)$. As a common feature we find the same overall behaviour for all material sets: The growth rates increase for small $k$ and reach a plateau for larger values of $k$.

In an attempt to understand the pattern formation of the sedimenting

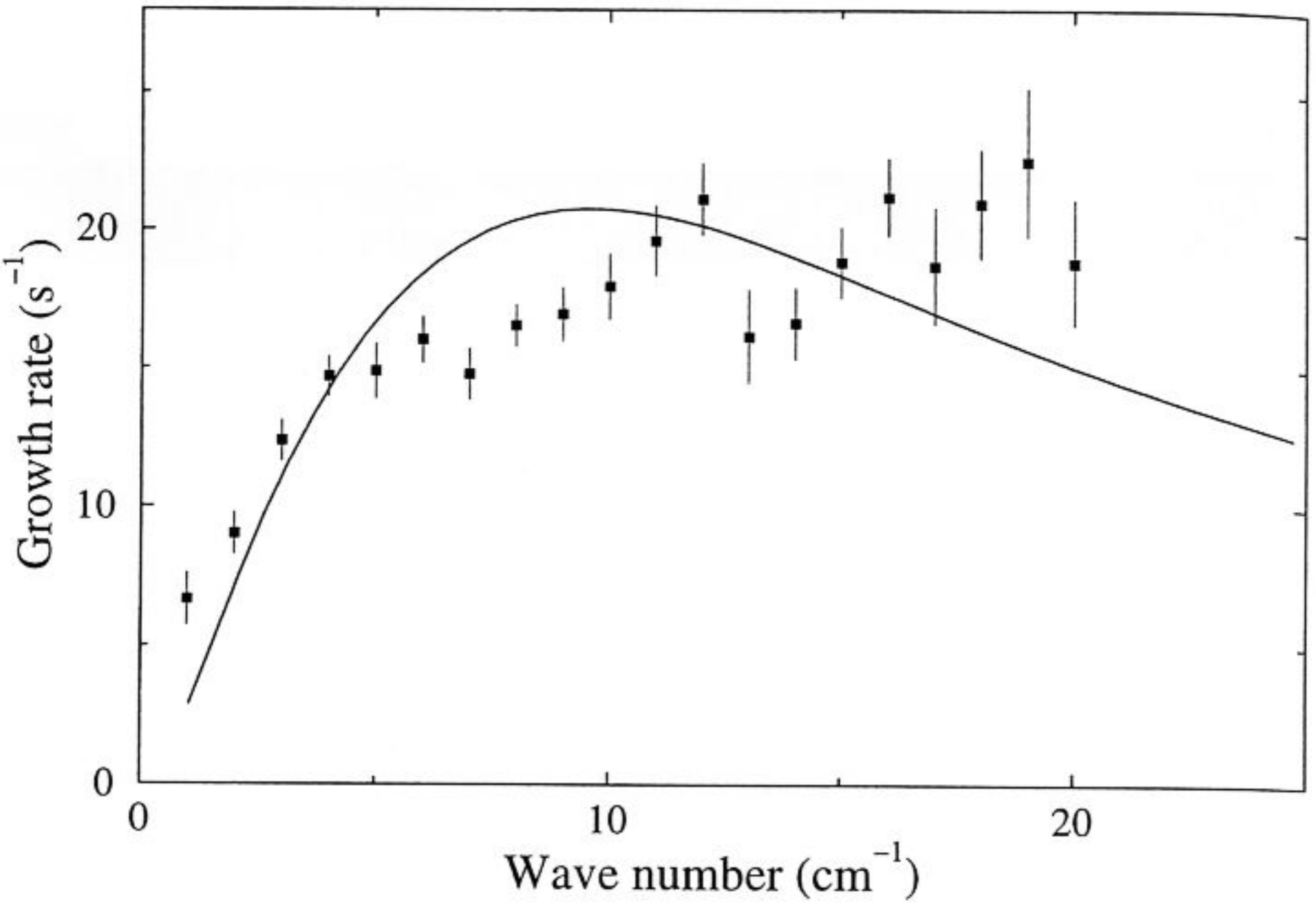


**Fig. 34.** Comparison of the experimental dispersion relation with theory. The square dots are the mean values of 42 experiments. The error bars give the standard deviation of the mean value. The solid line is yielded by a least square fit of the function obtained by a linear stability analysis.

suspension we considered a two–fluid model, where the suspension is seen as one fluid with a higher density than water, the second fluid. Within this model, our experiment is very reminescent of a classical hydrodynamic instability — the Rayleigh–Taylor instability. It occurs when a more dense fluid is stratified over a less dense one. The interface between the fluids is unstable, and the growth rate of a disturbance is a characteristic function of the wavelength and the fluid parameters. Following this idea, we have compared the experimentel dispersion relation with the results of a linear stability analysis of the two–fluid problem (Lange et al. 1998). The suspension is treated as a Newtonian fluid with a time dependent density, the initial density is set to be equal to that of the sedimented sand layer. The viscosity of the suspension is taken as a fit parameter. Under the assumption of vanishing surface tension a viscosity of about 100 times that of water is found. However, the theory is two–dimensional, while in the experiment due to the long rotation-time a

three–dimensional flow ensues, which affects the appearing patterns. In addition, we feel that there is a strong need of more precise measurements of the volume fraction of the falling suspension in order to enhance the quality of the quantitative comparison.

To our knowledge there is only one other publication examining Rayleigh-Taylor instabilities with suspensions (Didwania and Homsy 1981). These authors were not able to measure any growth rates or dispersion relations. There are also two–dimensional numerical simulations of a sedimenting particle front (Manwart and Schwarzer 1998). As the growth law for the amplitudes of the power spectrum the authors find:

$$A(t) = at + \frac{a}{b}\exp(-bt) + c \tag{6}$$

This result is confirmed by an linear stability analysis where the density is taken to be constant in time. However, for our experimental data the exponential growth gives the better fit. It is obvious that additional work is needed in order to understand the nature of the pattern formation during sedimentation.

## 3.3 Summary and Outlook

We presented a number of experiments and numerical simulations suitable for quantitative comparison with theoretical descriptions of granular matter. Especially in the case where only a few particles were involved, we found a remarkable agreement with the numerical and analytical models. For most of the experiments presented here, however, a quantitative comparison has not yet been achieved. We expect to see a lot of progress within the next few years especially due to numerical methods. An overview on these methods is provided in the appendix.

## 3.4 Acknowledgement

CMD & GHR gratefully acknowledge the invitation of the "Particle Science and Technology Group" of M. Nakagara at Colorado School of mines to conduct the experiment on axial segregation, which was performed with the help of J. L. Moss. The Magdeburg Group would like to thank many members of the European TMR-network on "Patterns, Noise and Chaos" for stimulating discussions and enthusiastic support. This work was supported by the Deutsche Forschungsgemeinschaft through Re 588/11 and Ri 826/1 within the Schwerpunktprogramm on "Strukturbildung in dissipativen kontinuierlichen Systemen: Theorie und Experiment im quantitativen Vergleich".

# Appendix: Numerical methods for simulating the dynamics of granular materials

Since there is no general theory for granular matter, *numerical simulations* are a useful tool for investigating idealized systems. Here they can provide a deeper insight into the systems. In numerical simulations we are looking for a passage from microscopic laws to macroscopic behaviour, i.e. the prediction of characteristic length and time scales. A big issue is the size of the investigated system. In order to model a realistic system at least $10^5$ particles have to be used. Even though granular particles in vacuum only interact when they collide, since the particles are large enough not to feel the Van der Waals forces, it is a numerically very intensive job and can only be done with todays high performance computers. For the dynamics of granular media it is essential that the interaction is *dissipative* and *nonlinear*. Various numerical techniques have been developed to address the difficulties in simulations of the dynamics of granular matter.

## Monte Carlo Method

One widely used numerical technique to study particle motions is the so–called *Monte Carlo* method. The name stems from the extensive use of random numbers in the calculations which are used to find new particle positions which minimize the potential energy of the system. This method was introduced into the field of granular materials more than 10 years ago to study the size segregation of binary mixtures undergoing vertical vibrations (Rosato et al. 1986, Rosato et al. 1987). Hard spheres were used with a normal restitution coefficient of zero to avoid an increase in potential energy. It was successful in stressing the geometrical effects of the process. A scaling law, relating the segregation velocity to the amplitude of shaking and to the diameter ratio of the particles, was found as well (Devillard 1990). It also served in testing a segregation model in a ternary system (Rosato et al. 1991).

## Cellular Automata

The use of *cellular automaton* models to study granular materials dates back to the introduction of the concept of *self-organized criticality*, where sand pile avalanche statistics were used as one example (Bak et al. 1987). In these models space is discretized into cells which have the size of the particles and can either be occupied or empty. The particle dynamics are modeled by a set of particle collision rules which apply when certain conditions are fulfilled, i.e. the local surface angle (slope) exceeds a threshold value. Theses rules were later refined by deriving them from experiments to study the segregation process (Fitt and Wilmott 1992) during particle outflow from two-dimensional

hoppers. It is also possible to choose collision rules which require the system to fulfill the Navier-Stokes equations, which is then called *lattice-gas* automaton (Flekkøy and Herrmann 1993). This seems to be a promising starting point to model granular materials when the rules are modified to include the important aspects of gravity, dissipation and static friction.

### Method of steepest descent

This deterministic model, which is capable of dealing with a very large number of particles, was first described by Jullien et al. (1992). It is motivated by the method of ballistic deposition and should be understood as a *toy-model* to study the geometrical effects in granular materials. Particles follow the path of steepest descent and undergo a sequence of *rolling* and *falling* steps before they reach a local surface minimum. New particle contacts are treated as completely inelastic collisions. This model was used to model the segregation process in the growing heap of a pile with an impressive $10^7$ and more particles (Meakin and Jullien 1992). The original model was extended by incorporating the exact form of the external excitation by Baumann et al. (1994) to study particle size segregation in rotating drums and was renamed *bottom-to-top-restructuring*.

### Molecular Dynamics (Granular Dynamics or Discrete Element Method)

The aforementioned methods have several limitations: (i) No physical time scale enters the models since the collision time is assumed to be zero, therefore a direct connection of the update time and the physical time is missing which greatly reduces the scope of these approaches. (ii) These models are capable to study mostly geometrical effects. To overcome these difficulties and limitations, another method is most widely used to model the dynamics of granular materials called *discrete element method* (DEM) which is essentially a molecular dynamics method including the particle history (Cundall and Strack 1979).

Here, each particle $i$ is approximated by a sphere with radius $R_i$, sketched in Fig. 35 and the wall is treated as a particle with infinite mass and radius. Only contact forces during collisions are considered and, depending on the material we want to simulate, the particle can or cannot rotate. For an example: in contrast to glass beads mustard seeds are slightly aspherical, so they tend not to rotate easily and the approximation of non-rotating particles is used. Whenever two particles $i$ and $j$ are closer than the sum of their radii particle $j$ exerts a force on particle $i$ and vice versa. The total contact forces can be split up into:

– Elastic, repulsive contact force in normal direction

$$f_{\mathrm{el}}^{(ij)} = \tilde{Y}(m_{\mathrm{eff}}, r_{\mathrm{eff}}) \; ((R_i + R_j) - \mid \mathbf{r}_{ij} \mid)^{\alpha} \quad ,$$

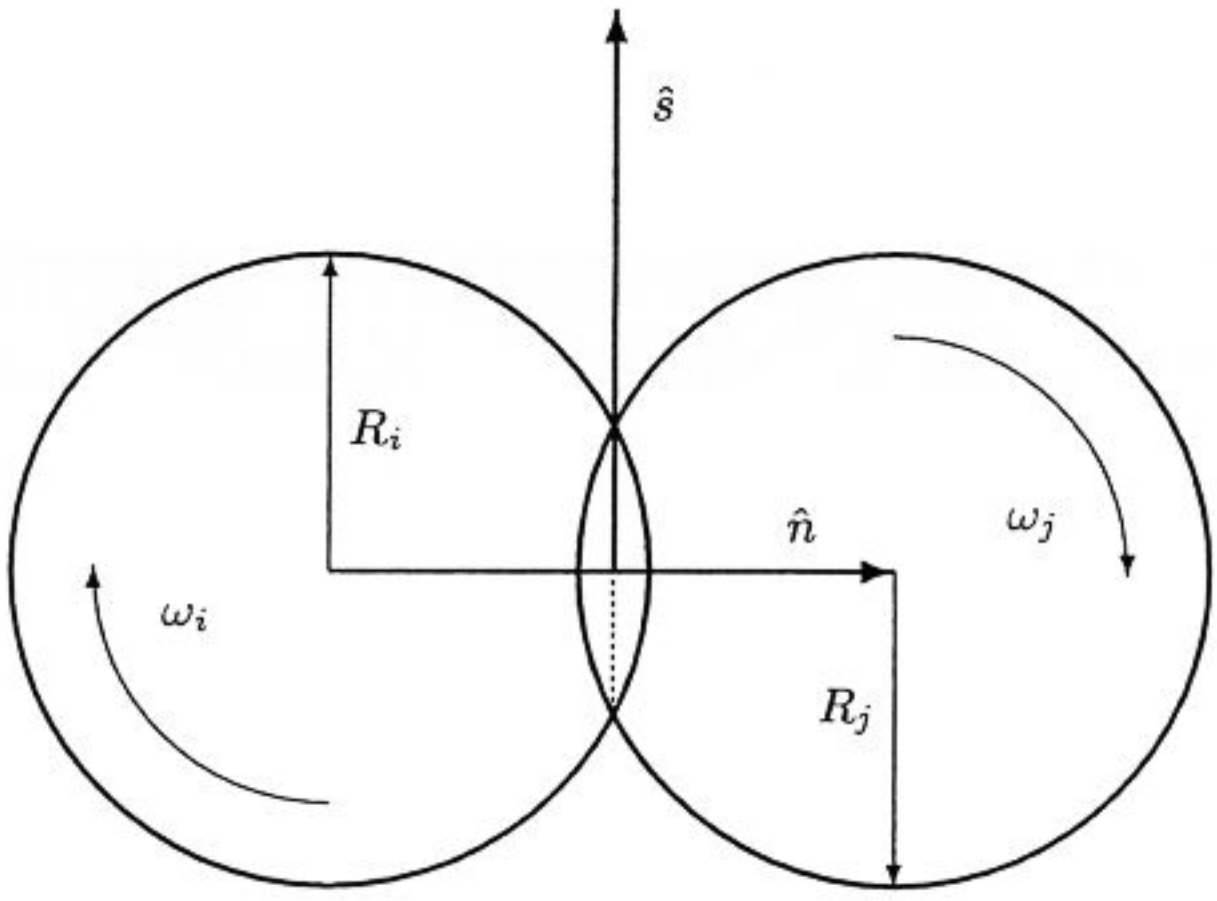


**Fig. 35.** Coordinate system during particle-particle collisions.

where $\tilde{Y}$ is the Young modulus of the investigated material and $|\mathbf{r}_{ij}|$ the distance between the centers of mass of particle $i$ and particle $j$.
For $\alpha = 1$ we get a Hooke like force and for $\alpha = 1.5$ the Hertzian contact force.

- Dissipation in normal direction

$$f_{\text{diss}}^{(ij)} = -\tilde{\gamma}(m_{\text{eff}}, r_{\text{eff}})\, \mathbf{v}_{ij} \cdot \hat{n} \ ,$$

$\tilde{\gamma}(m_{\text{eff}}, r_{\text{eff}})$ is the dissipation coefficient and is determined by the coefficient of restitution $\epsilon_{res}$. $\mathbf{v}_{ij} = \mathbf{v}_i + (\boldsymbol{\omega}_i \times \hat{n}) - (\mathbf{v}_j + (\boldsymbol{\omega}_j \times (-\hat{n})))$ denotes the relative velocity of the two colliding particles at the contact point, see Fig. 35. .

- Frictional forces in shear direction

1. Static friction (with static friction we get a finite angle of repose):

$$f_{\text{fric}}^{(ij)} = -k_s \int \mathbf{v}_{ij} \cdot \hat{s}(t) dt \ .$$

   For the static shear force, we put upon contact a linear spring between the two particles which results in a restoring force, i.e. the friction is proportional to the displacement of the original contact points.
2. Dynamic friction:

$$f_{\text{fric}}^{(ij)} = -\gamma_s \mathbf{v}_{ij} \cdot \hat{s}(t) \ .$$

   This is a viscous friction where the force is proportional to the relative velocity.

Both tangential forces are limited by the Coulomb criterion which states that the magnitude of the tangential force cannot exceed the magnitude of the normal force multiplied by the friction coefficient $\mu$. Therefore, if the restoring force would be larger than Coulomb's frictional force we switch to the friction with Coulomb's Law and we get:

$$f_{\text{shear}}^{(ij)} = \text{sign}(f_{\text{fric}}^{(ij)})\ \min(f_{\text{fric}}^{(ij)}, \mu \mid \mu f_{\text{el}}^{(ij)} + f_{\text{diss}}^{(ij)} \mid) \ .$$

The model parameters $(\tilde{Y}, \tilde{\gamma}, k_s(\gamma_s), \mu)$ have the following physical interpretation: $\tilde{Y}$ is related to the material stiffness, $\tilde{\gamma}$ to the energy loss during collisions (in experiments measured via the restitution coefficient) and the pair $k_s(\gamma_s)$ and $\mu$ controls the energy loss and static friction in the shear direction, e.g. via the surface roughness (Foerster et al. 1994). Commonly, $\mu$ is referred to as the Coulomb friction coefficient.

A detailed discussion of the different force laws is given by Schäfer et al. (1996), and a review of different applications using granular dynamics is given by Ristow (1994).

A technique very similar to the discrete element method are event driven simulations in which a variable time step is used which is well suited for dilute systems (Luding et al. 1994).

## References


Allen M. P., Tildesley D. J. (1990): *Computer Simulation of Liquids* (Clarendon Press, Oxford 1990)

Bagnold R. A. (1954): Experiments on a Gravity-free Dispersion of Large Solid Spheres in a Newtonian Fluid Under Shear. Proc. R. Soc. **225**, 49–63

Bak P., Tang C., Wiesenfeld K. (1987): Self-organized criticality: an explanation of $1/f$ noise. Phys. Rev. Lett.**59**, 381–384

Batchelor G. K., Green J. T. (1972): Determination of the bulk stress in a suspension of spherical particles to order $c^2$. J. Fluid Mech. **56**, 401–427

Batchelor G. K. (1977): The effect of Brownian motion on the bulk stress in suspension of spherical particles. J. Fluid Mech. **83**, 97–117

Baumann G., Janosi, I., Wolf D. E. (1994): Particle trajectories and segregation in a two-dimensional rotating drum. Europhys. Lett.**27**, 203–208

Bizon C., Shattuck M. D., Swift J. B., McCormick W. D., Swinney H. L. (1998): Patterns in 3d vertically oscillated granular layers: simulation and experiment. Phys. Rev. Lett.**80**, 57–60

Bridgewater J. (1976): Fundamental powder mixing mechanisms. Powder Technol.**15**, 215–236

Brown R. L. (1939): The fundamental principles of segregation. J. Inst. Fuel.**13**, 15–19

Cantelaube F., Bideau D. (1995): Radial segregation in a 2d drum: an experimental analysis. Europhys. Lett.**30**, 133–138

Choo K., Molteno T. C. A., Morris S. W. (1997): Traveling granular segregation patterns in a long drum mixer. Phys. Rev. Lett. **79**, 2975–2978

Clément E., Rajchenbach J. (1991): Fluidization of a Bidimensional Powder. Europhys. Lett. **16**, 133–138

Clément E., Duran J., Rajchenbach J. (1992): Experimental study of heaping in a two–dimensional "sandpile". Phys. Rev. Lett. **69**, 1189–1192

Clément E., Rajchenbach J., Duran J. (1995): Mixing of a granular material in a bidimensional rotating drum. Europhys. Lett.**30**, 7–12

Cooke W., Warr S., Huntley J., Ball R. (1996): Particle size segregation in a two-dimensional bed undergoing vertical vibration. Phys. Rev. E **53**, 2812–2822

Cundall P., Strack O. D. L. (1979): A discrete numerical model for granular assemblies. Géotechnique **29**, 47–65

Das Gupta S., Khakar D. V., Bathia S. K. (1991): Axial segregation of particles in a horizontal rotating cylinder. Chem. Engineering Science **46**, 1513–1517

Devillard P. (1990): Scaling behaviour in size segregation ("Brazil Nuts"). J. Phys. France **51**, 369–373

Didwania A. K., Homsy G. M. (1981): Rayleigh-Taylor Instabilities in Fluidized Beds. Ind. Eng. Chem. Fundam. **20**, 318–323

Dippel S., Luding S. (1995): Simulation on size segregation: Geometrical effects in the absence of convection. J. Phys. I France **5**, 1527–1537

Donald M. B., Roseman B. (1962): Mixing and demixing of solid particles. Br. Chemical Engineering **7**, 749–753

Dury C. M., Ristow G. H. (1997): Radial segregation in a two-dimensional rotating drum. J. Phys. I France **7**, 737–745

Dury C. M., Ristow G. H. (1998): Competition of Mixing and Segregation in Rotating Cylinders. subm. to Phys. Fluids

Einstein A. (1906): Eine neue Bestimmung der Moleküldimensionen. Ann. Phys. **19**, 289–306

Einstein A. (1911): Berichtigung zu meiner Arbeit: Eine neue Bestimmung der Moleküldimensionen. Ann. Phys. **34**, 591–592

Esipov S. E., Pöschel T. (1997): The granular phase diagram. J. Stat. Phys. **86**, 1385–1395

Evesque P., Rajchenbach J. (1989): Instability in a sand heap. Phys. Rev. Lett. **62**, 44–46

Evesque P. (1992): Shaking dry powders and grains. Contemporary Physics **33**, 245–261

Fitt A. D., Wilmott P. (1992): Cellular-automaton model for segregation of a two-species granular flow. Phys. Rev. A **45**, 2383–2388

Flekkøy E. G., Herrmann H. J. (1993): Lattice Boltzmann models for complex fluids. Physica A **199**, 1–11

Foerster S. F., Louge M. Y., Chang H., Allia K. (1994): Measurements of the collision properties of small spheres. Phys. Fluids **6**, 1108–1115

Gallas J. A. C., Herrmann H. J., Sokołowski S. (1992): Molecular dynamics simulation of powder fluidization in two dimensions. Physica A **189**, 437–446

Grossmann E.L., Zhou T., Ben-Naim E. (1997): Towards granular hydrodynamics in two dimensions. Phys. Rev. E **55**, 4200–4206

Hill K. M., Kakalios J. (1995): Reversible axial segregation of rotating granular media. Phys. Rev. E **52**, 4393–4400

Ichiki K., Hayakawa H. (1995): Dynamical simulation of fluidized beds: Hydrodynamically interacting granular particles. Phys. Rev. E **52**, 658–670

Janssen H. A. (1895): Versuche über Getreidedruck in Silozellen. Z. Verein Deutsch. Ing. **93**, 1045–1049

Jaeger H. M., Knight J. B., Liu C. H., Nagel S. (1994): What is shaking in the sandbox? MRS Bulletin **19**, 25

Jaeger H. M., Nagel S. R., Behringer R. P. (1996): The Physics of Granular Materials, Physics Today **49**, 32

Jaeger H. M., Nagel S. R., Behringer R. P. (1996): Granular solids, liquids, and gases. Rev. Mod. Phys. **68**, 1259–1273

Jenike W. (1964): Why bins don't flow. Mech. Engineering **5**, 40–43

Johanson J. R. (1978): Particle segregation ...and what to do about it. Chem. Engineering **8**, 183–192

Julien P., Lan Y., Raslan Y. (1997): Experimental mechanics of sand stratification. In: Behringer R. P., Jenkins J. T. (eds.): *Powders & Grains 97* (Balkema, Rotterdam), 487–490

Jullien R., Meakin P., Pavlovitch A. (1992): Three-dimensional model for particle-size segregation by shaking. Phys. Rev. Lett. **69**, 640–643

Knight J., Jaeger H., Nagel S. (1993): Vibration-induced size seperation in granular media: The convection connection. Phys. Rev. Lett. **70**, 3728–3731

Lange A., Schröter M., Scherer M. A., Engel A., Rehberg I. (1998): Fingering Instability in a Water-Sand Mixture. submitted to Euro. Phys. J. B

Lee J. (1995): Scaling behaviour of granular particles in a vibrating box. Physica A **219**, 305–326

Liffman K., Metcalfe G., Cleary P. (1997): Convection due to horizontal shaking. In: Behringer R. P., Jenkins J. T. (eds.): *Powders & Grains 97* (Balkema, Rotterdam), 405–408

Luding S., Herrmann H. J., Blumen A. (1994): Simulation of twodimensional arrays of beds under external vibrations: Scaling behaviour. Phys. Rev. E **50**, 3100–3108

Luding S., Clément E., Blumen A., Rajchenbach J., Duran J. (1994): The onset of convection in molecular dynamics simulations of grains. Phys. Rev. E, **50**, R1762–R1765

Makse H. A., Cizeau P., Stanley H. E. (1997): Possible stratification mechanism in granular mixtures. Phys. Rev. Lett. **78**, 3298–3301

Manwart C., Schwarzer S. (1998): Response analysis for the early stage of sedimentation processes. Preprint.

Meakin P., Jullien R. (1992): Simple models for two and three dimensional particle size segregation. Physica A **180**, 1–18

Melo F., Umbanhowar P., Swinney H. L. (1994): Transition to parametric wave patterns in a vertically oscillated granular layer. Phys. Rev. Lett. **72**, 172–175

Melzer A., Homann A., Piel A. (1996): Experimental investigation of the melting transition of a plasma crystal. Phys. Rev. E **53**, 2757–2766

Metcalfe G., Shinbrot T., McCarthy J. J., Ottino J. M. (1995): Avalanche mixing of granular solids. Nature **374**, 39–41

Nakagawa M. (1994): Axial segregation of granular flows in a horizontal rotating cylinder. Chem. Engineering Science - Shorter Communications **49**, 2540–2544

McNamara S., Young W.R. (1996): Dynamics of a freely evolving, two-dimensional granular medium. Phys. Rev. E **53**, 5089–5100

Pätzold R. (1980): Die Abhängigkeit des Fließverhaltens konzentrierter Kugelsuspensionen von der Strömungsform: Ein Vergleich der Viskosität in Scher- und Dehnströmungen. Rheo. Acta **19**, 322–344

Ristow G. H. (1994): Granular dynamics: a review about recent molecular dynamics simulations of granular materials. In: Stauffer D., (ed.): *Annual Reviews of Computational Physics I* (World Scientific, Singapore), 275–308

Ristow G., Straßburger G., Rehberg I. (1997) Phase Diagram and Scaling of Granular Materials under Horizontal Vibrations. Phys. Rev. Lett. **79**, 833–836

Rosato A. D., Lan Y., Wang D. T. (1991): Vibratory particle size sorting in multicomponent systems. Powder Technol. **66**, 149–160

Rosato A. D., Prinz F., Strandburg K., Swendsen R. (1986): Monte carlo simulation of particulate matter segregation. Powder Technol. **49**, 59

Rosato A. D., Strandburg K. J., Prinz F., Swendsen R. H. (1987): Why the Brazil Nuts are on top: Size segregation of particulate matter by shaking. Phys. Rev. Lett. **58**, 1038–1040

Rosenkranz D.E., Pöschel T. (1997) Recurrent swelling of horizontally shaken granular material. Preprint cond-mat / 9712108.

Schäfer J., Dippel S., Wolf D. E. (1996): Force schemes in simulations of granular materials. J. Phys. I France **6**, 5–20

Scherer M. A., Buchholtz V., Pöschel T., Rehberg I. (1996): Swirling granular matter: from rotation to reptation. Phys. Rev. E **54**, R4560–R4563

Scherer M. A., Mahr T., Engel A., Rehberg I. (1997): Granular dynamics in a swirled annulus. subm. to Phys. Rev. E

Scherer, M. A. (1998): *Der Schwenkeffekt: Experimentelle Untersuchungen zur granularen Dynamik* (Dissertation, Universiät Magdeburg, Magdeburg)

Sela N., Goldhirsch I., Noskowicz S. H. (1996): Kinetik theoretical study of a simple sheared two-dimensional granular gas to Burnett order. Phys. Fluids **8**, 2337–2353

Spahn F., Schwarz U., Kurths J. (1997): Clustering of Granular Assemblies with Temperature Dependent Restitution under Keplerian Differential Rotation. Phys. Rev. Lett. **78**, 1596–1599

Standish N. (1985): Studies of size segregation in filling and emptying a hopper. Powder Technol. **45**, 43–56

Straßburger G., Betat A., Scherer M. A., Rehberg I. (1996): Pattern Formation by Horizontal Vibration of Granular Material. In: Wolf D. E., Schreckenberg M., Bachem A. (eds.): *Traffic and Granular Flow* (World Scientific), 329-333

Taguchi Y. H. (1993): $k^{-5/3}$ Power Spectrum in Powder — Turbulent flow in a Vibrated Bed: Numerical Results. Europhys. Lett. **24**, 203–209

Vanel L., Rosato A. D., Dave R. (1997): Rise–times regimes of a large sphere in vibrated bulk solids. Phys. Rev. Lett. **78**, 1255–1258

Warr S., Huntley J. M., Jacques G. T. H. (1995): Fluidization of a two–dimensional granular system: Experimental study and scaling behaviour. Phys. Rev. E **52**, 5583–5595

Williams J. C. (1976): The segregation of particulate materials. A review. Powder Technol. **15**, 245–251

Yokoyama T., Tamura K., Usui H., Jimbo G. (1996): Simulation of ball behavior in a vibration mill in relation with its grinding rate – effects of fractional ball filling

and liquid viscosity. In: Forssberg E. (ed.): *Proceedings of the Eighth Symposium on Comminution, Stockholm, 1994* (Elsevier, Amsterdam) 413–425

Zik O., Levine D., Lipson S. G., Shtrikman S., Stavans J. (1994): Rotationally induced segregation of granular materials. Phys. Rev. Lett. **73**, 644–647